Geochimica et Cosmochimica Acta 359 (2023) 57–70

Contents lists available at ScienceDirect

Geochimica et Cosmochimica Acta

journal homepage: www.elsevier.com/locate/gca

Impacts of nepheloid layers and mineralogical compositions of oceanic margin sediments on REE concentrations and Nd isotopic compositions of seawater

Yi Huang [a], Christophe Colin [a,*], Zhifei Liu [b], Eric Douville [c], Arnaud Dapoigny [c], Frederic Haurine [a], Qiong Wu [d], Andrew Tien-Shun Lin [e]

[a] Université Paris-Saclay, CNRS, GEOPS, 91405 Orsay, France
[b] State Key Laboratory of Marine Geology, Tongji University, Shanghai 200092, China
[c] Laboratoire des Sciences du Climat et de l'Environnement, LSCE/IPSL, UMRCEA CNRS-UVSQ, Université Paris-Saclay, F-91191 Gif-sur-Yvette, France
[d] College of Oceanography, Hohai University, 210098 Nanjing, China
[e] Department of Earth Sciences, National Central University, Jhongli 32001, Taiwan

ARTICLE INFO

Associate editor: Franco Marcantonio

Keywords:
Seawater
Nd isotope composition
REE contents
Boundary exchange
Nepheloid layers

ABSTRACT

Nepheloid layers and turbidity currents transport large quantities of detrital sediments to deep-sea basins. Locally they may control seawater – detrital particle interactions and modify dissolved REE concentrations and εNd distributions of the oceanic margin. However, to date, such processes have been poorly documented, especially in oceanic margins characterized by contrasted mineralogical compositions. Dissolved REEs and εNd from three water stations collected in the northern South China Sea (SCS) close to the Taiwanese deep-sea canyons have been analyzed, with the aim of determining the influence of nepheloid layers and mineralogical composition of lithogenic inputs on dissolved REE and εNd distributions in the ocean. Results indicate that the most radiogenic εNd value (-2.5 ± 0.2), observed at about 400 m, corresponds to the inflow of North Pacific Intermediate Water (NPIW) into the SCS. When compared with previously published Nd isotope, our current study suggests that the εNd value of NPIW which enters the SCS (from 300 to 800 m water depth) is not modified by unradiogenic sediments off the southern margin of Taiwan Island, whereas they become less radiogenic along the margin of eastern China due to Nd exchange with unradiogenic sediments (between −10.2 and −12.6) from the tropical soils of Chinese rivers basins. We have proposed that pedogenetic minerals from Chinese tropical soils modify the Nd isotopic compositions of seawater more efficiently than fresh detrital minerals resulting from very high rates of physical erosion on Taiwan Island. The MREE/MREE*, La/Sm and La/Yb ratios in nepheloid layers indicate that lateral transportation of lithogenic material within the water column can preferentially adsorb LREE compared to MREE and HREE through the scavenging process. However, this process has a negligible impact on seawater εNd of the northern SCS. At the bottom of several water stations, a negative excursion of εNd values, associated with an increase in MREE/MREE* ratios and a decrease in La/Sm ratios, suggests a remineralization flux resulting from the dissolution of Mn oxides during early diagenesis of deep-sea sediments.

1. Introduction

Dissolved neodymium (Nd) isotopic composition (expressed in epsilon units, εNd) is heterogeneous in the ocean due to lithogenic inputs from continents and the shorter residence time of Nd (about ~500–1000 yrs Tachikawa et al., 1999, 2003; Arsouze et al., 2009; Rempfer et al., 2011; van de Flierdt et al., 2016) compared to the global turnover time of the thermohaline circulation (about ~1500 yrs, Broecker and Peng 1982). Oceanic basins acquire different isotopic Nd compositions through lithogenic inputs characterized by different εNd depending on the age and nature of the outcropping rocks and sediments on continents (Goldstein and Hemming, 2003; Frank, 2002). Away from the continental margins, εNd is considered as a "quasi-conservative" proxy in the ocean and is widely used to trace changes in water mass provenance and mixing of water masses both at the present time and in the past at different time scales (e.g. Piepgras and Wasserburg, 1980;

* Corresponding author.
E-mail address: christophe.colin@universite-paris-saclay.fr (C. Colin).

https://doi.org/10.1016/j.gca.2023.08.026
Received 11 January 2023; Accepted 30 August 2023
Available online 1 September 2023
0016-7037/© 2023 Elsevier Ltd. All rights reserved.

Nozaki and Alibo, 2003; Piotrowski et al., 2005; Jeandel et al., 2007; Dubois-Dauphin et al., 2017; Wu et al., 2017; Colin et al., 2019; Duhamel et al., 2020; Fuhr et al., 2021).

There is a general increase in the dissolved εNd of bottom water of the ocean along the thermohaline circulation, from −15 in the North Atlantic to −4 in the North Pacific, which is not associated with a subsequent general increase in the Nd concentrations (Frank, 2002). This decoupling of Nd concentrations and εNd values in the ocean was initially referred to as the "Nd paradox" (Goldstein and Hemming, 2003). Today it is assumed that the water masses acquire their εNd values from downwelling surface water through lithogenic inputs by rivers and wind transport, "boundary-exchange" processes that occur at the continental margin (Lacan and Jeandel, 2005; Jeandel et al., 2007; Jeandel, 2016; Wilson et al., 2012; Tachikawa et al., 2017), reversible scavenging in the water column (Bertram and Elderfield, 1993; Tachikawa et al., 2003; Siddall et al., 2008, Wang et al., 2021; Robinson et al., 2023) and benthic flux which releases Nd from pore fluids during early diagenesis of deep-sea sediments (Abbott et al., 2015, 2019, 2022; Haley et al., 2017; Du et al., 2022). These processes, which figure in the interplay between particulates and seawater, are still not fully understood and further investigations are required to quantify their respective roles in the Nd budget of the ocean (Robinson et al., 2021, Wang et al., 2022). In addition, several previous studies infer that the reversible scavenging between dissolved and particulate phases could be dependent on the mineralogy of the lithogenic input to the ocean and/or the state of chemical weathering of the lithogenic material (Blanckenburg and Nagler 2001, Hindshaw et al., 2018, Larkin et al., 2021). Consequently, physical erosion and chemical weathering of rocks, combined with the efficiency of sediment transfer to the oceanic margin, may impact the reactivity of the labile fraction and its exchange with seawater (Larkin et al., 2021). Nevertheless, some important issues regarding the mineralogical fractions that can exchange Nd with seawater are still unsolved.

Marginal seas, associated with strong lithogenic inputs, are key areas for studying the interaction between seawater and detrital particulates. Along the continental shelf or slope, nepheloid layers induced by high velocity deep-sea currents, occur widely. These are turbid layers containing significantly more suspended particles than the adjacent layers in oceans (Tian et al., 2022). It has been shown that the high amounts of resuspended particles in benthic nepheloid layers enhance exchange between particles and seawater, which influences Nd isotopes of bottom waters (Gardner et al., 2018, Blaser et al., 2020). Several studies have also identified a decrease in Nd concentrations of seawater collected in benthic nepheloid layers (Casse et al., 2019), and link the depleted or sometimes elevated Nd concentrations of bottom water to potential scavenging by resuspended particles in benthic nepheloid layers (Stichel et al., 2015; Morrison et al., 2019; Wang et al., 2021). However, the dissolved REE behaviors in benthic nepheloid layers are not yet constrained. Nevertheless, the resuspended particles in the intermediate nepheloid layers are rarely investigated even though they have the potential to significantly modify the Nd isotope signature of seawater in the water column. Thus, the dissolved REE and εNd distributions collected in the nepheloid layers are crucial to better understanding the "boundary exchange" process along the continental slope.

The South China Sea (SCS) is an ideal area to evaluate the effect of lithogenic input on the dissolved Nd cycle of the ocean. The SCS receives sediments from numerous surrounding major Asian rivers (e.g., the Pearl River, the Red River, and the Mekong River) characterized by markedly more unradiogenic εNd values (from −13 to −11; Wei et al., 2012) than those of the Pacific Ocean water masses which enter the SCS via the Luzon Strait (εNd from −2.5 to −4, Wu et al., 2015). More specifically, suspended sediments from southwest Taiwan represent the largest source discharged directly into the northern SCS, with a total load of 176 Mt/yr carried by several small rivers (Dadson et al., 2003). Typhoon-induced floods commonly trigger turbidity currents that flow within submarine canyons off Taiwan (Zhang et al., 2018). They also generate and maintain the large nepheloid layers on the shallow continental slope to the southwest of Taiwan (Geng et al., 2018; Jia et al., 2019). This massive sediment discharge may represent a major source of unradiogenic lithogenic Nd to the SCS and could significantly influence the dissolved REE budget in the northern SCS, as has recently been observed in marginal seas at the outlets of large river basins (Yu et al., 2017a; Pham et al., 2019; Garcia-Solsona and Jeandel 2020). Previous records of dissolved REEs in the SCS have shown that particles from rivers surrounding the SCS are dissolved and could provide additional Nd to the surface water (Amakawa et al., 2000; Alibo and Nozaki 2000; Wu et al., 2015, 2022). However, the contribution of suspended sediment discharge from Taiwan's rivers and of nepheloid layers to the distribution of dissolved REE concentrations and εNd, especially of intermediate- and deep-water masses, has not yet been investigated in detail.

Here, we present the dissolved REE concentrations and εNd values of seawater samples collected at three water stations in the deep-sea canyon system off the southern coast of Taiwan. When compared with previous εNd values obtained on seawater samples collected along the eastern margin of China (Wu et al., 2015; 2022), the εNd results presented here permit us i) to record the dissolved Nd concentrations and isotope compositions in the northern SCS on the pathway of North Pacific Intermediate Water (NPIW) and Pacific Deep-Water (PDW) entering the SCS; ii) to evaluate the impact of intermediate and benthic nepheloid layers on dissolved REE concentrations and εNd distributions and iii) to assess the effect of "boundary exchange" along continental margins characterized by contrasted mineralogical sediment compositions.

2. Seawater samples and hydrological settings

35 seawater samples, each of 12L, were collected at three stations (HS1, HS6 and HS10) located close to the deep-sea canyons of southern Taiwan during the HydroSed cruise, on board *R/V Marion Dufresne*, in July 2018 (Table S1, Fig. 1). Station HS1 is located on the western levee of Gaoping Canyon, whereas station HS6 is in a more distal position relative to this canyon. Station HS10 is located on the eastern bank of the Penghu Canyon (Fig. 1). As station HS6 was collected in the same water masses as stations HS1 and HS10 and in an intermediate position between both stations, only the lower part of the water column has been collected to constrain lithogenic inputs from bottom sediments. Seawater samples were collected, and the relevant hydrographic parameters (conductivity, potential temperature, and depth) determined using a Sea-Bird SBE 911plus CTD-Rosette system equipped with a transmissivity-sensor, a O_2-sensor, a fluorimetry sensor and 24 Niskin bottles.

The Luzon Strait, with a depth of about 2400 m, is the only deep-sea channel connecting the SCS to the western Pacific Ocean (Philippine Sea) (Li and Qu 2006; Qu et al., 2006) (Fig. 1a and 1b). The water column in the Luzon Strait presents a strongly stratified structure due to the inflow of surface and deep waters to the SCS and the outflow of intermediate water masses to the Philippine Sea (Yuan 2002; Tian et al., 2006; Gan et al., 2016; Zhu et al., 2019). In the surface layer, the North Pacific Tropical Water (NPTW, 19–20 °C, 34.85‰–35.25‰; Qu et al., 1999; Suga et al., 2000) flows into the SCS in the northern part of the Luzon Strait (Fig. 1c). It is locally driven by the seasonal reversal of wind direction that induces a cyclonic gyre in winter and an anticyclonic gyre in summer (Fig. 1, Wyrtki 1961).

For water stations HS1 HS6 and HS10, the relatively low salinity values, from 33.6‰ to 34.3‰, above 100 m is mainly due to the freshwater discharge from Taiwanese rivers and heavy monsoon rainfall over the northern SCS (Figs. 2a and 3). A salinity maximum of 34.7, associated with a potential temperature of 18.5 °C, is identified in our stations at a depth of 160 m (Fig. 2a and 2b). This water mass with slightly higher salinity is termed South China Sea Tropic Water (SCSTW, 17-19 °C, 34.6‰–34.7‰) (Xie et al., 2011). The water mass at

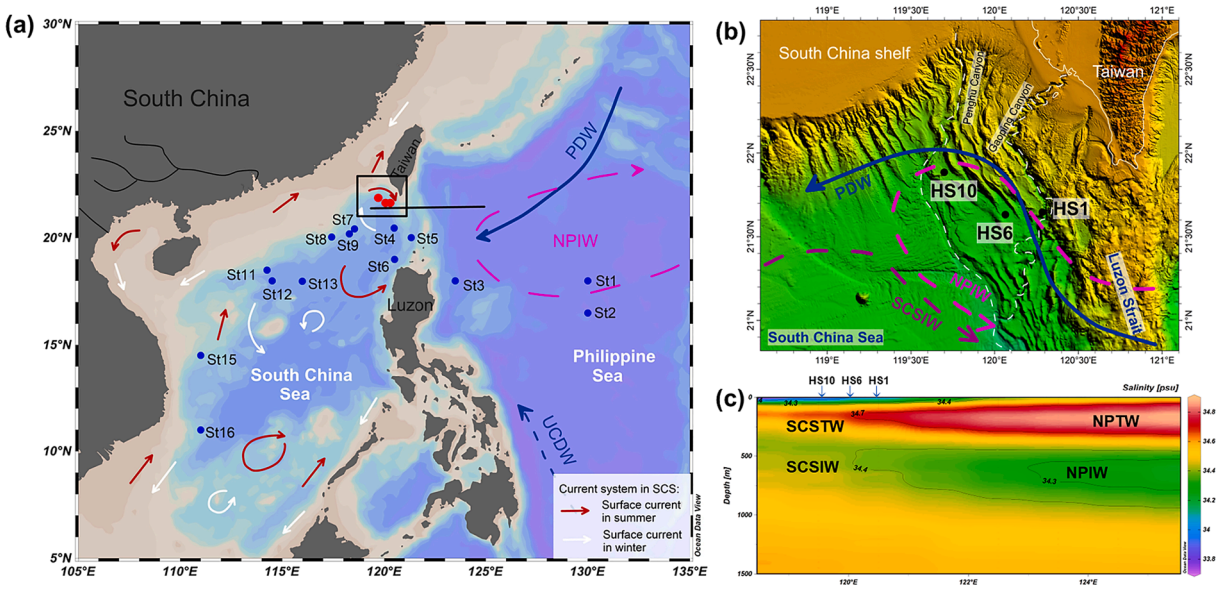

Fig. 1. Sampling map of seawater stations in the SCS and western Pacific Ocean. The red circles represent the HydroSed sites in this study, the blue circles indicate other seawater stations mentioned in the discussion (Wu et al., 2015). The circulations are based on (Kawabe et al., 2009; Kawabe and Fujio (2010); You, 2003; Liu et al., 2016). The topographic map (b) is an enlargement of the solid square indicated in (a), it shows the specific locations of seawater sites and two deep-sea canyons (Gaoping Canyon and Penghu Canyon) in northern Taiwan. (c) The salinity contours along the transect in the Luzon Strait. The salinity data were taken from the World Ocean Atlas 2013.

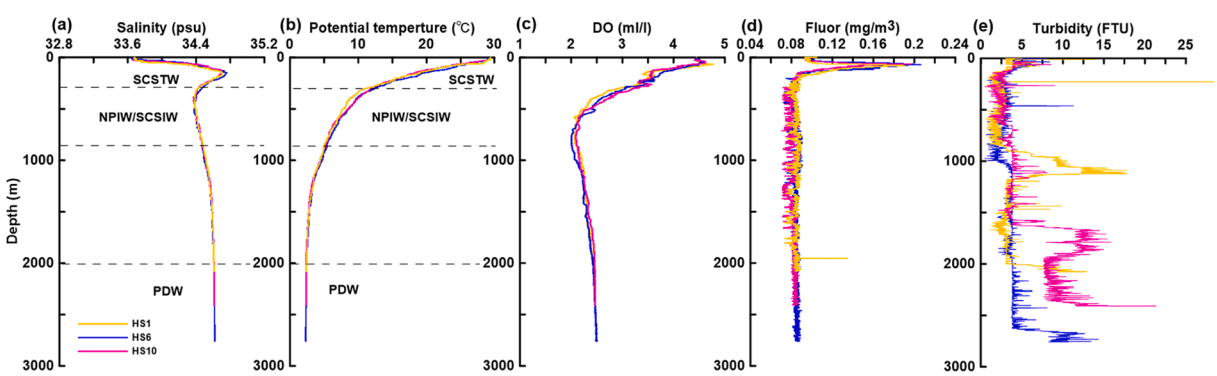

Fig. 2. Vertical profiles of salinity (a), potential temperature (b), dissolved oxygen (c), Fluor concentration (d) and turbidity (e) at stations HS1, HS6 and HS10.

intermediate depth (300–800 m) is characterized by a slightly lower salinity 34.37‰–34.45‰ and a potential temperature of 5.8–11.2 °C (Fig. 2a and 2b). This reflects a mixing of North Pacific Intermediate Water (NPIW, 34‰–34.3‰; You, 2003) and South China Sea Intermediate Water (SCSIW, 34.45‰–34.5‰; Chen et al., 2001; Xie et al., 2011) (Fig. 3).

As demonstrated by hydrographic analysis and numerical models (Qu et al., 2000; Fang et al., 2009; Gan et al., 2016), the SCSIW flows eastward to the Philippine Sea at deeper depths of between 500 and 1500 m to compensate for the inflow of Pacific water in the surface layer (e.g., Chao et al., 1996; Qu et al., 2000; Tian et al., 2006). This implies that the NPIW does not intrude as far into the SCS as the NPTW. However, recent studies indicate that the intermediate water exchange between the SCS and the Philippine Sea is very complex with strong seasonal variability. During summer, there is a westward inflow of NPIW in the northern part of the strait and an eastward outflow of SCSIW in the southern part; the flow pattern across the strait is reversed in winter (Yang et al., 2010; Xie et al., 2011; Zhu et al., 2019).

In the deeper layer (>2000 m), salinity (34.59‰~34.62‰) and potential temperature (2.3 ~ 2.5 °C) display narrow ranges that are identical to the water mass properties of the Pacific Deep Water (PDW, 34.62‰, 2.1 °C) in the Philippine Sea at about 2000 m (Figs. 2a, 2b and 3) (Broecker et al., 1986; Chen et al., 2001; Wu et al., 2015, 2022), suggesting a westward inflow of PDW in the Luzon Strait. The PDW sinks after crossing the Luzon Strait (Wyrtki 1961) and to compensate for this descending movement, intense vertical mixing occurs in the SCS. Therefore, the renewal of the SCS deep water is rapid, about 30 to 100 yrs (Li and Qu 2006; Qu et al., 2006). The SCS Contour Current system refers to a deep-water current (2000–2500 m) that transports a vast amount of sediment counter-clockwise within the SCS (Qu et al., 2006; Wang et al., 2011; Zhao et al., 2015).

The studied sites are located within the channel-levee system of southern Taiwan, which is characterized by frequent turbidity currents (Zhang et al., 2018; Fig. 1). Transmissivity data obtained on sites HS1, HS6 and HS10 allow us to identify several intermediate and benthic nepheloid layers. Nepheloid layers were identified between 900 and 1200 m and at the bottom (below 2000 m) at site HS1, and between 1600 and 1900 m and at the bottom (below 2400 m) at site HS10 (Fig. 2e). A benthic nepheloid layer was observed only at the bottom at site HS6 (below 2600 m), as we might expect given its more distal location relative to the active Gaoping Canyon. This site, HS6, should be less influenced by the horizontal advection of large volumes of sediments by turbidity currents and/or contourite currents.

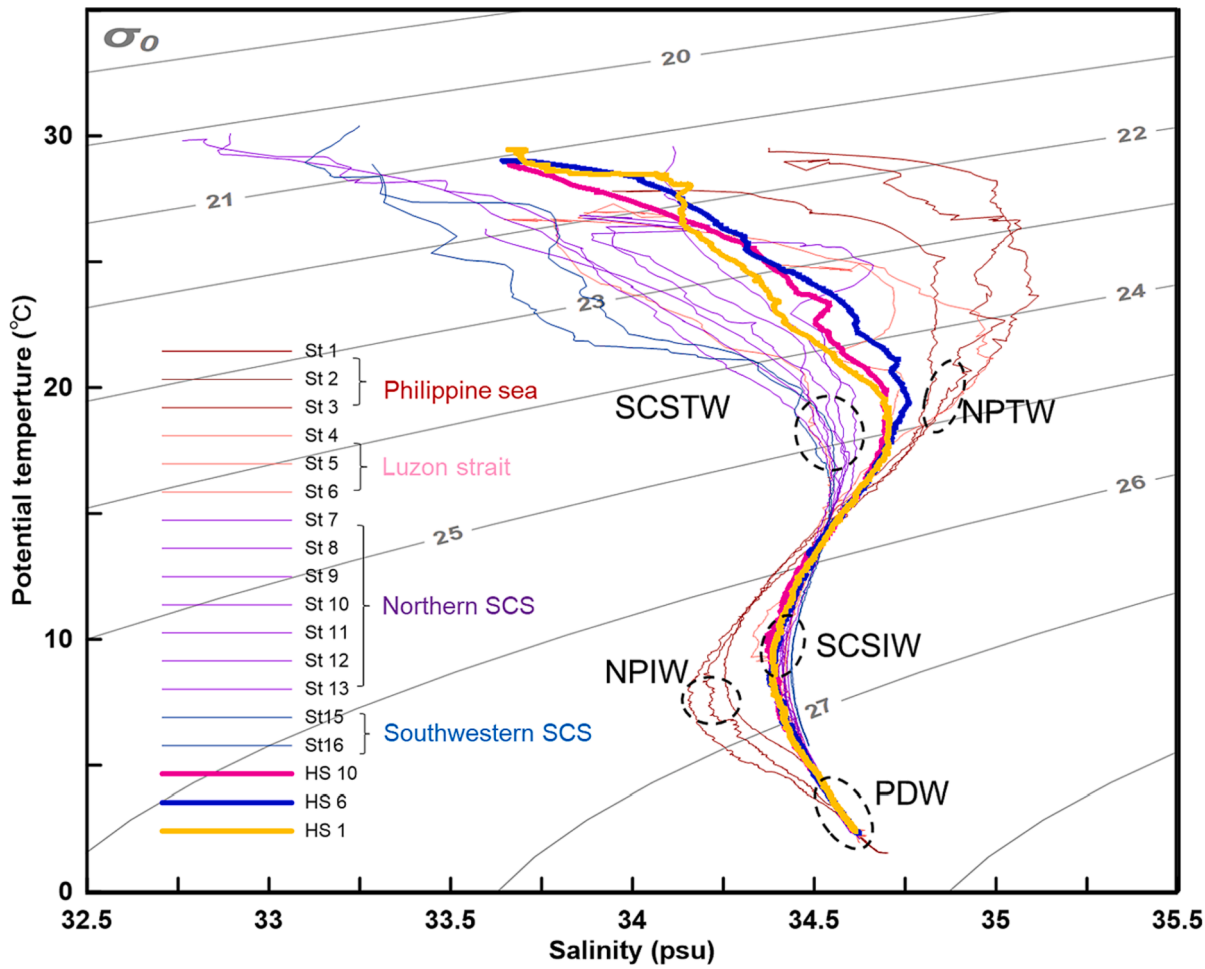

Fig. 3. Salinity versus potential temperature diagrams of three water stations investigated in this study and other seawater stations in the SCS and western Pacific (Wu et al., 2015). Water masses are labeled as follows: Pacific Deep Water-PDW, Upper Circumpolar Deep Water - UCDW, North Pacific Intermediate Water - NPIW, South China Sea Intermediate Water - SCSIW, North Pacific Tropical Water - NPTW, South China Sea Tropical Water - SCSTW.

3. Methods

All seawater samples were filtered onboard, using AcroPak 500 capsule filters (0.8–0.45 μm), and then transferred to ~10-12L acid cleaned (1 M HCl) bottles. Seawater was acidified to a pH of less than 2 with supra-pure 6 N HCl immediately after sampling in accordance with GEOTRACES recommendations (van de Flierdt et al., 2012). Nd was extracted and purified from the seawater matrix following the analytical procedures described in detail by Lacan and Jeandel (2001). In brief, seawater REEs were first pre-concentrated using SepPak Classic C18 cartridges loaded with a HDEHP/H2MEHP complexing agent, and the REEs were then purified using a cationic resin (AG50W-X8). Finally, an *Eichrom Ln-Spec* resin was used to extract and purify Nd following the method described in detail by Copard et al., (2010).

The $^{143}Nd/^{144}Nd$ ratios of all purified Nd fractions were analyzed using the *ThermoScientific Neptune^{Plus}* multi-Collector Inductively Coupled Plasma Mass Spectrometer (MC-ICP-MS) hosted at the *Laboratoire des Sciences du Climat et de l'Environnement (LSCE)* at the University Paris-Saclay (PANOPLY's analytical facilities, France). The isotopic compositions were measured at a Nd concentration of 10 to 15 ppb. During the analytical sequence, every group of three samples was bracketed with analyses of Jndi-1 standard, which is characterized by certified values of 0.512115 ± 0.000006 (Tanaka et al., 2000). Mass-dependent fractionation was corrected relative to $^{146}Nd/^{144}Nd$ of 0.7219 by applying an exponential-fractionation law. The deviation between results and certified values of JNdi was inferior to 0.5 εNd units for all the εNd results presented in this study. The external reproducibility (2σ) calculated for analytical sequences from repeated measurements of JNdi-1 standards (n = 20) was 0.18 epsilon units. Analytical uncertainties obtained in this study fully conform to previous εNd results obtained by the GEOPS Laboratory under the calibration exercise involving 15 international laboratories dedicated to Nd isotopes in seawater (van de Flierdt et al., 2012). Total procedural blank values (including the Nd pre-concentration step with C18 cartridge) were <100 pg, representing less than 0.5% of the Nd signal measured for seawater samples characterized by the lowest Nd concentration analyzed in this study.

Dissolved REE concentrations were analyzed on 250 mL seawater samples (split seawater samples from on-board filtering and acidification) using a single collector sector field high resolution inductively coupled plasma mass spectrometer (HR-ICP-MS) *Thermo Element XR* hosted at the *Laboratory GEOPS* (PANOPLY's analytical facilities at the *University Paris-Saclay*, France), following the method described in detail by Wu et al., (2015). Briefly, an ultra-pure iron hydroxide solution and a spike solution enriched in ^{141}Pr and ^{169}Tm were added to each sample with contents around 10–50 times higher than the REE concentrations in samples. After 48 h of equilibration, the pH was adjusted to ~8 by the addition of ultraclean NH_4OH (Ammonia solution 28%), leading to the formation of iron hydroxides, which, in turn, efficiently scavenge REEs out of the seawater samples. The REE co-precipitated fractions were then separated from the remaining solution through several centrifugations and careful rinsing with Milli-Q water and several drops of

NH_4OH. The residues were re-dissolved in ultra-pure 3 N HNO_3 and evaporated to dryness. The dried samples were re-dissolved in 2 mL 8 N HNO_3 and 50 μL HF to get rid of any silica gel that might precipitate during Fe co-precipitation. After drying, REEs were separated from the matrix using anion exchange columns (AG1-X8 resin, mesh 100–200). During analytical sequences using HR-ICP-MS, REE concentrations were corrected for any sensitivity drift of the machine by using internal standard monitoring. The added ^{141}Pr and ^{169}Tm spikes allowed the calculation of the REE extraction step recovery (higher than 92%) and finally REE concentrations by considering the initial Pr and Tm contents in the samples. REE data was calculated with uFREASI software (Tharaud et al., 2015). The accuracy of the determination of REE concentrations was validated by analysis of two geological standards, BCR-2 and BHVO2, prepared at various dilutions with a deviation that was systematically lower than 5%. Blank contributions are considered negligible for all REEs since analysis of chemical blanks (spike solutions before and after chemistry) revealed an REE signal that was systematically lower than 1% (most often less than 1‰) compared to REE signals measured for each sample. Finally, our measurements were characterized by analytical uncertainties that were systematically below 5% (2σ) for all REEs. Such uncertainties integrate the accuracy of calibrations, the addition of a spike solution and its measurement, and, finally, the external reproducibility.

4. Results

4.1. Dissolved REE concentrations

Dissolved REE concentrations from all of the analyzed seawater stations are reported in Table S2 and Fig. 4, S1. The range of REE concentrations is comparable to previously published values for seawater in the SCS (Alibo and Nozaki 2000; Wu et al., 2015) and other ocean basins (Amakawa et al., 2009; Grasse et al., 2017). With the exception of Ce, vertical profiles of all dissolved REE concentrations display a similar behavior with maximum concentrations (eg. 34 pmol/kg for Nd) at the surface and a minimum at subsurface (eg. 8 pmol/kg for Nd at 140 m) (Fig. 4, S1). Below this minimum the concentrations progressively increase towards the bottom… At station HS1, Ce concentrations decreases from 9 pmol/kg to 3 pmol/kg from the surface to 500 m, then increase gradually to 8–12 mol/kg at 1500 m, with little variations in deeper waters. This pattern is specific to station HS1.

Dissolved REE concentrations normalized to Post Archean Australian Shale (PAAS; McLennan 1989) reveal environmental fractionation between the light (LREE; La, Ce, Pr, and Nd), middle (MREE; Sm, Eu, Gd, Tb and Dy) and heavy REEs (HREE; Ho, Er, Tm, Yb, and Lu). PAAS normalized REE concentrations display similar patterns for all stations with a pronounced Ce negative anomaly and a progressive increase of the REE concentrations from the lightest to the heaviest REE (Fig. S2). This is a typical seawater PAAS normalized REE pattern, because trivalent HREEs are strongly bound by stable carbonate complexes in seawater and are less likely to be scavenged into particles compared to LREE in the water column, thus leaving a HREE-enriched seawater (Bertram and Elderfield 1993). The Ce anomaly is the result of the poor solubility of its oxidative state (+IV) and preferential scavenging of this element (Sholkovitz et al., 1992; Jeandel et al., 2013).

Some specific REE ratios ($La/Sm = La_N/Sm_N$, $La/Yb = La_N/Yb_N$, $Ce^* = Ce_N/(2*Pr_N-Nd_N)$, $MREE/MREE^* = (Gd_N + Dy_N)/(Yb_N + Nd_N)$; N denotes normalization to PAAS) are used to assess the individual fractionation differences (Grenier et al., 2018; Pham et al., 2019). La/Sm and La/Yb ratios imply a fractionation difference between LREE and MREE, LREE and HREE, respectively. La/Sm ratios range from 0.5 to 1.1 in the water column (Fig. 5a). La/Sm ratios are low at the surface and

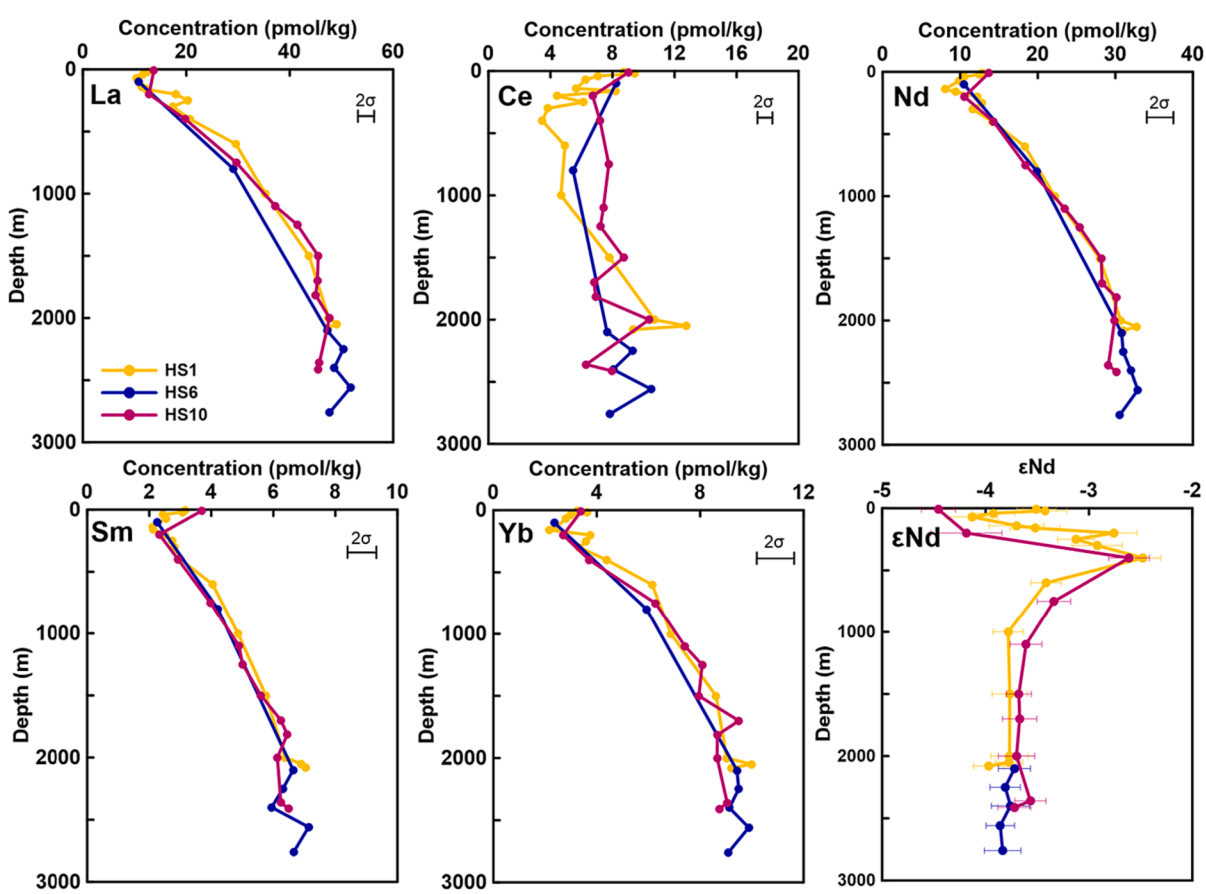

Fig. 4. Vertical profiles of dissolved La, Ce, Nd, Sm, Yb concentrations and εNd values at stations HS1, HS6 and HS10.

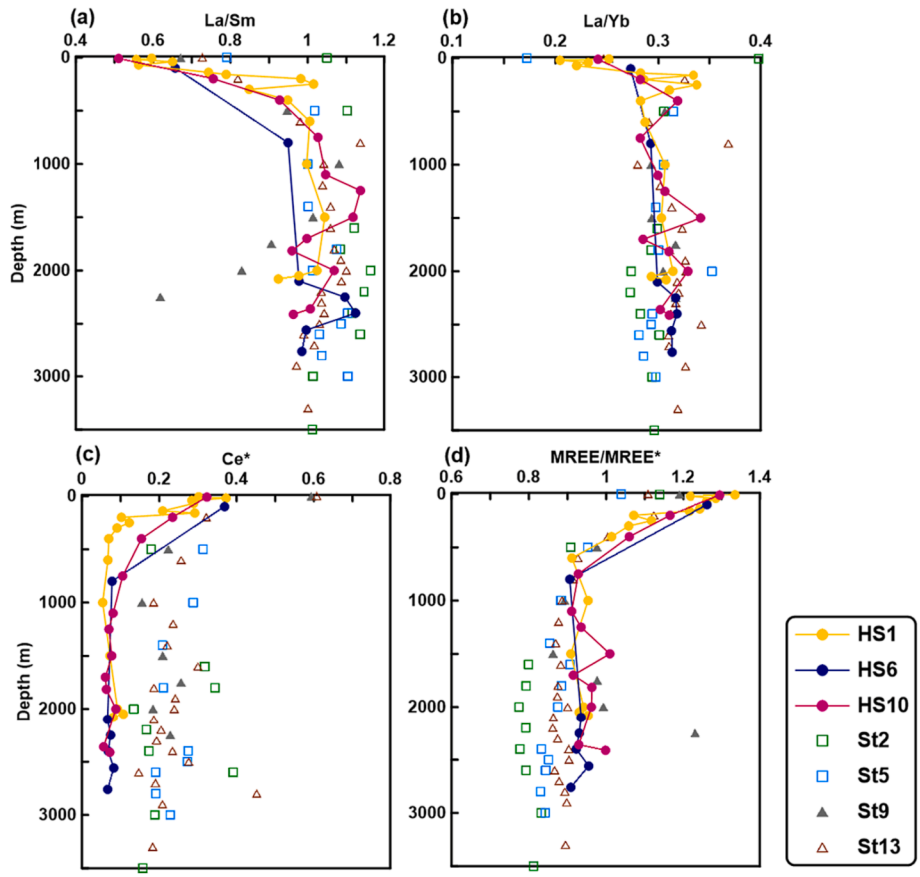

Fig. 5. Vertical profiles of La/Sm (a), La/Yb (b), Ce* (c) and MREE/MREE* (d) ratios in the northern SCS (HS1, HS6, HS10, St7, St8 and St9), Luzon Strait (St5), Philippine Sea (St2) (data of Stations St2, St5, St7, St8 and St9 are cited from Wu et al., 2015).

increase gradually to a depth of 800 m. It displays a reduced variation in the intermediate nepheloid layers (1600–1900 m) in station HS10 and at bottom (stations HS1 and HS10), while an increased shift was recognized in the 2200–2500 m in station HS6. La/Yb ratios are low in the upper 150 m and remain stable at a value of 0.3, with slight variations, at greater water depth in station HS1 and HS6, a reduced ratios are recognized in the intermediate nepheloid layers in HS10 (Fig. 5b). Ce* are 0.4 at surface and decrease to a depth of 300 m, then they remain stable at a value of 0.1 (Fig. 5c). MREE/MREE* ratio indicates an enrichment of MREE. The MREE/MREE* ratio is around 1.3 at the surface and decreases to around 0.9 below 500 m with slight variations (Fig. 5d).

4.2. Nd isotope compositions

The Nd isotope compositions of the seawater samples are reported in the Table S1 and Fig. 4. The vertical profiles of εNd from the three water stations located off southern Taiwan are similar (Fig. 4). Surface seawater has the lowest εNd values, with values of −4.5 ± 0.2 at 10 m for site HS10 and −4.1 ± 0.3 at 70 m for site HS1. The most radiogenic εNd values, observed at a depth centered around 400 m, are −2.5 ± 0.2 and −2.6 ± 0.2 in stations HS1 and HS10, respectively. Below this layer,

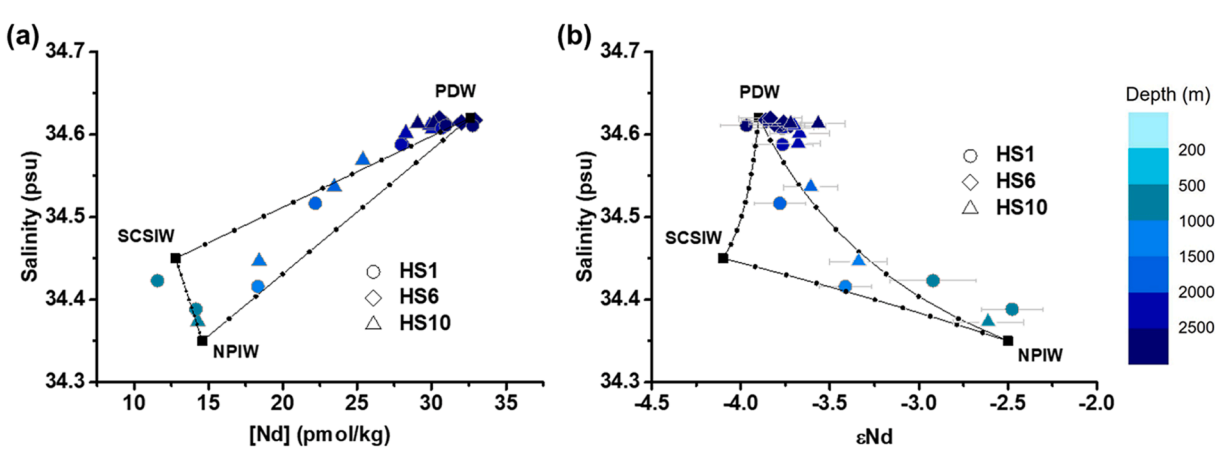

Fig. 6. Mixing relationships of major water masses in the SCS based on salinity versus Nd concentration (a) and salinity versus εNd (b) of seawater in stations HS1, HS6 and HS10.

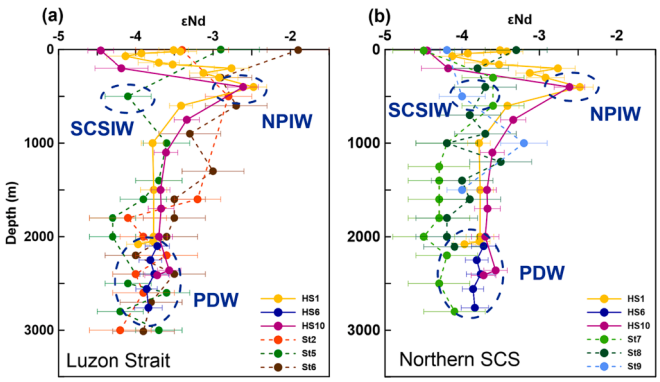

Fig. 7. Comparison of εNd from stations HS1, HS6 and HS10 of this study and Northern SCS (St7, St8 and St9) (a), the Luzon Strait (St5 and St6) and the Philippine Sea (St2) (b). (results of St5-St9 and St13 are from Wu et al., 2015).

the εNd values decrease to around −3.8 and remain constant below 1000 m (average of −3.8 ± 0.2, n = 4 for HS1 and average of −3.6 ± 0.2, n = 5 for HS10). At the bottom of stations HS1 (14 m above surface sediments) and HS10 (18 m above surface sediments), there is a slight negative shift. The εNd values below 2000 m in station HS6 stay constant at −3.9 ± 0.1 to −3.8 ± 0.2, and the slight negative shift observed at sites HS1 and HS10 is not observed in the bottom sample from station HS6 (24 m above surface sediments).

5. Discussion

5.1. Vertical distributions of dissolved REE concentrations and εNd in Southern Taiwan

In the northern SCS, the elevated fluorescence at ~50 m associated with elevated turbidity and dissolved oxygen content reflects an enrichment in organic compounds at these depths (Chen et al., 2011) (Fig. 2d). REE results revealed low concentrations in this highly productive sub-surface layer, with a minimum at around 140 m depth (e.g, Nd concentration is 8.63 pmol/kg) below the fluorescence and turbidity maximum (Fig. 4). This suggests that the presence of particles and organic compounds cause a higher rate of REE scavenging and adsorption in this sub-surface layer of the water column. This has been already observed in the Northern and Southern Atlantic Ocean (Stichel et al., 2015; Wang et al., 2021). Specifically, the formation of organic particles in the water column preferentially absorbs LREEs dissolved in seawater. Thus, this process is reflected by low La/Sm and La/Yb ratios of seawater at this depth (Fig. 5a and 5b). For the surface layer, the lower La/Sm and La/Yb ratios in the three studied stations (HS1, HS6 and HS10) compared to the same ratios in the Philippine Sea (St2; Wu et al., 2015) indicate that there are stronger biological activities in the northern SCS and that these dominate the REE fractionation at surface level.

Besides biological activities, the dissolution of riverine particles could provide additional REE to the surface water in northern SCS (Wu et al., 2022). The MREE/MREE* ratios of surface water for stations HS1, HS6 and HS10 range from 1.21 to 1.33 (Fig. 5d). Such MREE/MREE* ratios are slightly higher than the value in the Philippine Sea (1.16; St2). The MREE/MREE* ratios of dissolved material from Taiwanese rivers and dust inputs ranges from 2.8 to 3 (Chung et al., 2009) and from 1.13 to 1.19 (Li et al., 2013), respectively. Since aeolian dusts are considered to be insignificant compared to river sediments inputs in terms of terrigenous supplies to the northeastern SCS (Liu et al., 2010), we suggest that the REEs from the dissolution of Taiwanese river particles, are the major source of REEs to the surface seawater of the northern SCS, thus explaining the MREE/MREE* ratios described above.

The three studied stations (HS1, HS6 and HS10) are located on the direct pathway of western Pacific water masses that enter the northern SCS and are thus suitable for determining water mass exchanges between the SCS and the Philippine Sea. In the Philippine Sea, εNd values of the NPTW at surface and subsurface depths vary slightly, from −2.1 ± 0.3 to −3.4 ± 0.4 depending on the level of lithogenic input (Wu et al., 2015; Behrens et al., 2018). For the surface seawater collected in the northern part of the SCS, εNd values range from −3.4 ± 0.2 to −4.5 ± 0.2 in the upper 100 m (Fig. 4), suggesting a modification of the Nd isotopic composition of the NPTW entering the northern SCS. Higher dissolved REE concentrations and stronger Ce negative anomalies observed at stations HS1 and HS10, compared to those of the Philippine Sea (St2, St3), confirm a greater input of riverine sourced REEs and pronounced scavenging of Ce by detrital sediments (Figs. S3 and 5c). However, the surface water εNd values in stations HS1 and HS10 are not as negative as the dissolved εNd values of seawater collected in the northern SCS along the eastern margin of China (Fig. 7; from −5.3 ± 0.3 to ~−7.0 ± 0.3 for stations St.11, St.12 and St.13; Wu et al., 2015). This implies that surface water masses at stations HS1 and HS10 might be less modified by sediment inputs from Taiwanese rivers.

As previously deduced from local hydrological properties, the intermediate and deep seawater are greatly influenced by the water masses from the western Pacific (NPIW and PDW) and local modified water masses (SCSIW). Diagrams of salinity versus Nd concentrations and salinity versus εNd values are presented in Fig. 6 to evaluate the conservative characteristics of the εNd for water masses entering the SCS through the Luzon Strait. Since previous studies have demonstrated that the water masses in the Philippine Sea are strongly influenced by NPIW deriving from the north, rather than by AAIW originating from the south (Behrens et al., 2018; Fuhr et al., 2021), we do not take AAIW into account in our mixing curve. The values of three end-members (PDW, NPIW and SCSIW) are chosen from average values of water masses in the Philippine Sea (Wu et al., 2015; Behrens et al., 2018) and SCS (Wu et al., 2015; 2022), which can be taken to closely represent the water masses flowing at the studied sites (Table 1). All results obtained on seawater samples below 300 m are within the mixing line between the three end-members.

In stations HS1 and HS10, the intermediate waters (300–800 m) are located close to the NPIW endmember, rather than SCSIW (Fig. 6b). The εNd values (−2.5 ± 0.2 and −2.6 ± 0.2) observed at 400 m for stations HS1 and HS10 are similar to the εNd values of intermediate waters of the Philippine Sea (εNd = −2.8 ± 0.3, St2 at 500 m, Wu et al., 2015) (Fig. 7a). Moreover, seawater samples were collected in July, during the summer monsoon rainfall period which is associated with large discharges into the northern SCS of sediments with unradiogenic εNd values (Liu et al., 2016; Wei et al., 2012). It has been demonstrated that Nd isotopic compositions of surface and intermediate waters, down to a depth of more than 1000 m, may be greatly impacted by seasonal-controlled riverine inputs in marginal seas such as the Bay of Bengal (Yu et al., 2017). However, in regards to our study sites, this process seems not to cause a shift towards negative values for Nd isotopes of the intermediate water at stations HS1 and HS10. Consequently, the intermediate water masse from the northern SCS, close to the Luzon Strait,

Table 1
Water mass endmembers for the mixing curve in Figs. 7 and 9.

Water masses	Salinity	[Nd]	εNd	References
NPIW	34.35	14.6	−2.5 ± 0.3	Wu et al., 2015; Behrens et al., 2018
SCSIW	34.45	12.8	−4.1 ± 0.3	Wu et al., 2015; 2022
PDW	34.62	32.6	−3.9 ± 0.4	Wu et al., 2015; Behrens et al., 2018

seems to be mainly influenced by the NPIW, without any significant modification by local lithogenic inputs.

Below 1500 m, the deep-water masses are located close to the PDW endmember (Fig. 6). εNd values vary within a narrow range from −3.7 ± 0.2 to −4.0 ± 0.2. Such Nd isotopic compositions are also equivalent to the deep-water εNd values in the Philippine Sea (−4.1 ± 0.5; Wu et al., 2015) and in the North Pacific (from −4.2 to −3.2; Amakawa et al., 2004; Behrens et al., 2018; Fuhr et al., 2021). Such results confirm that the εNd of the PDW generally maintains its conservative character when it enters the SCS through the Luzon Strait. Moreover, mooring observation indicates that the PDW mixes vigorously with intermediate waters in the Luzon Strait (Tian et al., 2009; Zhou et al., 2023). Such intense vertical mixing and rapid turnover in the SCS (30–50 yrs; Li and Qu 2006) cause the slightly more radiogenic Nd isotopic compositions of deep water at stations HS1, HS6 and HS10 compared to the compositions of deep water in the northern SCS (Fig. 7b). This is supported by the fact that seawater results from 800 m and 1500 m lie well within the mixing curve between PDW and NPIW end-members in the salinity versus Nd concentration and salinity versus εNd diagrams (Fig. 6).

In summary, despite the fact that the εNd values of surface waters are slightly modified by local lithogenic discharge, the Nd isotope compositions of water at mid- and deep depth retain their conservative characteristics off southern Taiwan. The εNd values can thus be used with confidence to track the intrusion of Pacific water masses at intermediate and deep depths.

5.2. Spatial distributions of dissolved εNd of intermediate water masses in the northern SCS

Intermediate waters collected at stations St7, St8, St9 and St13 (Fig. 1) are characterized by more negative values (εNd = −3.6 ± 0.4 at 600 m in St7; εNd = −3.7 ± 0.4 at 600 m in St8; εNd = −4.0 ± 0.3 at 500 m in St9; εNd=- −3.2 ± 0.3 at 400 m in St13; Wu et al., 2015) than stations HS1 and HS10 (Fig. 7b). However, these stations are located to the southwest of stations HS1 and HS10 under the same current system which turns along the Northern margin of the SCS. Such results suggest that the εNd of intermediate water masses at a greater distance (St7, St8, St9 and St13) from the Luzon Strait are modified over the course of their circulation along the eastern China margin. Two mechanisms may explain this modification of the Nd isotopic signatures: 1/ vertical mixing of the NPIW with SCS deep-water characterized by relatively more negative εNd values (∼-4; Wu et al., 2015); 2/ boundary exchange of intermediate water masses with unradiogenic sediments (∼-12; Wei et al., 2012) of the northern margins of the SCS.

After the intrusion of the NPIW into the SCS, vertical mixing occurs between the NPIW (εNd of ∼-2.7) and the PDW (Tian et al., 2009), which is characterized by more negative values (∼-4; Wu et al., 2015). From the salinity versus εNd diagram (Fig. 8a and 8b) we can see that intermediate water masses (from 300 to 800 m) display a tendency toward the PDW end-member from the northern and southern Luzon Strait (HS1, HS10 and St6) to the eastern China margin (St7, St8, St9 and St13) with its concentration do not vary much. This shows that NPIW is gradually modified by vertical mixing of deep water after it enters the Luzon Strait. Station 5, collected in the central part of the Luzon Strait in winter, is characterized by the lowest εNd values and fits closely with the SCSIW end-member. This is in agreement with the situation of an outflow of the SCSIW to the Philippine Sea that has been observed for this part of the Luzon Strait during winter (Tian et al., 2006). In contrast, the samples from stations HS1 and HS10, collected during summer, indicate relatively "pure" NPIW that has intruded from the Philippine Sea. Such results indicate that Nd isotopic compositions have not been modified, at least off southern Taiwan.

We use a mixing model to predict the Nd isotopes of the intermediate water (between 300 and 800 m), supposing the added Nd isotopes result only from the upwelling of PDW from lower depths (Wang et al., 2021). We predict the ε_{Nd} using the following equation:

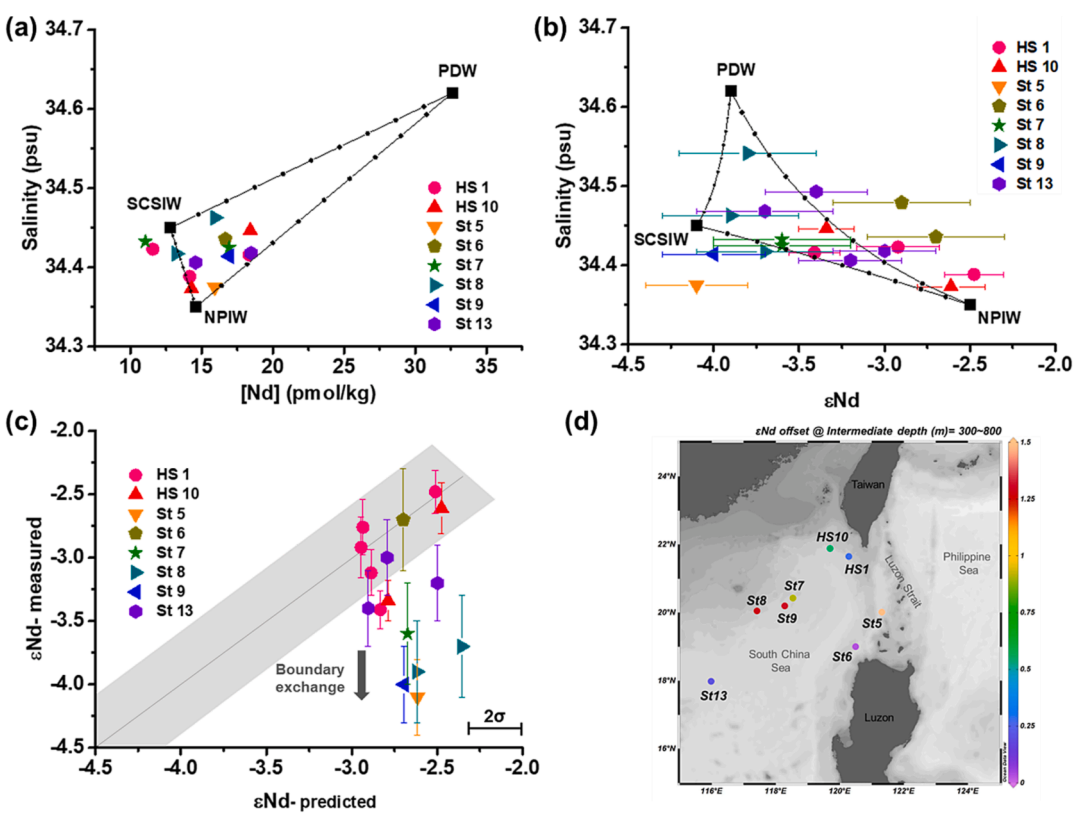

Fig. 8. Mixing relationships of major water masses at intermediate depth (300–800 m) in the SCS based on salinity versus Nd concentration (a) and salinity versus εNd values (b). (c) Measured εNd values versus predicted εNd values. (d) Spatial distribution of εNd offset. (results of St5-St9 and St13 are from Wu et al., 2015).

$$\varepsilon_{Nd}^{predicted} = \frac{[Nd]_{NPIW} * \varepsilon_{Nd}^{NPIW} + [Nd]_{add} * \varepsilon_{Nd}^{add}}{[Nd]_{measured}}$$

We take the SCS basin-scale view and suppose that the εNd values of intermediate water at 300–800 m are the result of vertical mixing of NPIW and water masses in lower depth; then once the εNd added is determined, the predicted Nd isotope compositions ($\varepsilon_{Nd}^{predicted}$) due to upwelling is related to the amount of Nd added ($[Nd]_{add} = [Nd]_{measured}$-$[Nd]_{NPIW}$). We take the maximum ε_{Nd}^{add} of −4 (εNd of PDW) for our calculation. The predicted εNd value results calculated using the above formula, versus the εNd values measured in the northern SCS are shown in Fig. 8c. The εNd results for stations St5, St7, St8 and St9 are more negative than the predicted results, suggesting that, apart from the vertical mixing, another source of Nd with negative εNd values needs to be taken into consideration.

The boundary exchange process can modify εNd values of intermediate water and thus may account for the εNd offset ($\varepsilon_{Nd}^{measured}$-$\varepsilon_{Nd}^{predicted}$). It is interesting that this offset becomes more pronounced for stations along the southwest margin of Taiwan (HS1 and HS10; offset < 0.5) to the eastern China margin (St7, St8 and St9; offset > 1.5) which will be discussed in the later sections (Fig. 8d).

5.3. The role of intermediate nepheloid layers in dissolved REE concentrations and εNd distributions

The re-suspended particles transported in nepheloid layers could act as a major source or sink for the REEs (Tian et al., 2022; Gardner et al., 2018), and their increasing exchanges with seawater are liable to impact the dissolved REE pattern and εNd. Nepheloid layers are widely distributed in the northern SCS (Geng et al., 2018; Jia et al., 2019) and could contribute significantly to the boundary exchange process. Intermediate nepheloid layers were observed at station HS1 from 900 to 1200 m, at station HS10 from 1600 to1900 m, at station St7 from 1000 to 1500 m and at station St 8 from 500 to 1000 m (Fig. 9, Wu et al., 2015). Except for station HS1, similar variations of La/Yb, La/Sm and MREE* are found in seawater samples collected in all intermediate nepheloid layers (Fig. 9). This suggests that similar processes dominate the REE fractionation in nepheloid layers in the northern SCS.

Seawater samples collected in intermediate nepheloid layers reveal slightly lower La/Sm, La/Yb and MREE/MREE* ratios in comparison with samples collected directly above and below. Allochthonous detrital particles are believed to preferentially adsorb LREEs and MREEs and precipitate authigenic Fe-Mn oxides (Gutjahr et al., 2007; Du et al., 2016). The decreased La/Sm, La/Yb and MREE/MREE* ratios can be related to comparatively greater scavenging of LREEs and MREEs by the detrital material which is transported laterally in the nepheloid layers (Fig. 10). This deep scavenging has been also observed in the north Atlantic oxygen minimum zone, where detrital materials result from aeolian dusts (Stichel et al., 2015). It supports the role of detrital materials as a sink of dissolved REE by scavenging at greater depth. We can conclude that the scavenging process dominates REE fractionation in the intermediate nepheloid layers of the northern SCS.

There is no change of La/Sm, La/Yb and MREE* in the intermediate nepheloid layer in station HS1. It could be related to stronger reversible scavenging in this station, suggested by lower Ce concentrations and stronger negative Ce anomaly in upper 1000 m (Figs. 4, 5c). This might obscure the variations in the intermediate nepheloid layer. A decrease of La/Yb and MREE can also be found outside the nepheloid layers (at around 2000 m in station St7 and bottom of St8). It might be some lateral advection of a water parcel that has been in contact with a nepheloid layer and transported the already depleted signal.

A slight decrease in Nd concentrations has been found in nepheloid layers (Fig. 9) where it has been linked to the removal of Nd from seawater by a process of scavenging by re-suspended particles. This scavenging has also been observed in the nepheloid layers along the coast of Papua New Guinea (Grenier et al., 2013), in the estuary and Gulf of St. Lawrence (Casse et al., 2019), along the coast of Iceland (Morrison et al., 2019) and in the southern Atlantic Ocean (Wang et al., 2021) where it causes a depletion of dissolved Nd concentrations (Gardner et al., 2018). However, there are no significant vertical variations in the dissolved εNd of nepheloid layers in the northern SCS, with the exception of the bottom of station St9 (Fig. 9), whereas the εNd values of sediment from the margins of Taiwan and China (from −10.2 to −12.6; Liu et al., 2016) are 6 to 8 epsilon units lower than PDW (εNd of −4). We can thus conclude that for stations HS1, HS10, St7 and St8 exchange between suspended sediments in nepheloid layers and seawater appears, in this case, to not significantly modify the Nd isotopic signatures of the water masses. One hypothesis to explain such lack of variations is that the particle dissolution rate of the labile phase of the suspended sediments cannot efficiently release Nd characterized by unradiogenic isotope compositions to the water column (Abbott, 2019). This suggests a potential control by the mineralogical compositions of the sediments transported in nepheloid layers. However, we cannot also exclude the possibility that suspended particles in the nepheloid layers become fully equilibrated with ambient seawater in the open ocean and therefore are no longer considered to be particle reactive (Stichel et al., 2020).

5.4. Impacts of detrital material mineralogy in Nd exchange with seawater

Water masses flowing along the southern margin of Taiwan and the eastern margin of China are influenced by the various river systems that transport sediments with contrasting mineral compositions to these margins (Liu et al., 2016). The mineral compositions of surface sediments collected at different depths along the margin of Taiwan (Liu et al., 2008) and of Eastern China (Liu et al., 2010) are shown in Fig. 11. Specifically, sediments from the southwest margin of Taiwan are dominated by minerals resulting from high rates of physical erosion, such as illite (more than 60%), while smectite and kaolinite account for less than 15% (Fig. 11a; Liu et al., 2008; 2016). Such mineralogy is associated with extremely high rates of physical erosion on Taiwan Island (Dadson et al., 2003; Liu et al., 2008). In the case of the margin of eastern China, minerals derive mainly from South China drainage systems (e.g., Pearl River), which are characterized by tropical soils resulting from stable tectonic conditions and intensive chemical weathering. The mineralogy of surface sediments from the margin of eastern China is thus characterized by low proportions of illite and chlorite, higher smectite contents (up to 50%) and higher illite crystallinity, especially at intermediate depth (200–1000 m) where NPIW intrudes into the SCS (Fig. 11b; Liu et al., 2010). The higher illite crystallinity (Fig. 11b) suggests a more pronounced state of weathering for illite deriving from tropical soils of the stable Chinese craton (Liu et al., 2016). Higher illite crystallinity values and smectite proportions on the eastern margin of China, compared to the southern margin of Taiwan, are coexistent with the modified intermediate water εNd values in the northern SCS (Fig. 11). This suggests that more pronounced states of weathering of minerals are likely to influence the dissolved Nd isotopes. This agrees with a previous study which suggests that chemical weathering of fresh rock under glacial conditions induces more exchange with seawater (Zhao et al., 2019). In addition, partial dissolution of detrital particles (such as smectite, amphibole and/or volcanic glass) or weathering of volcanic sediments have been demonstrated to modify εNd values of pore water (Du et al., 2022; Wang et al., 2022). All these studies suggest that smectite exchanges Nd with seawater more efficiently than illite or chlorite minerals. In the northern SCS, smectites derive mainly from the volcanic area of Luzon and to a lesser extent from chemical weathering of primary minerals in the soils of South China (Liu et al., 2016). More intense erosion and weathering of sedimentary rock enhances the reactivity of the labile fraction and its transfer to seawater (Larkin et al., 2021). Thus, pedogenic minerals (e.g., smectite, kaolinite, iron oxides and other pedogenic minerals) may play a major role in the Nd exchange between particulates and dissolved seawater (Fig. 10).

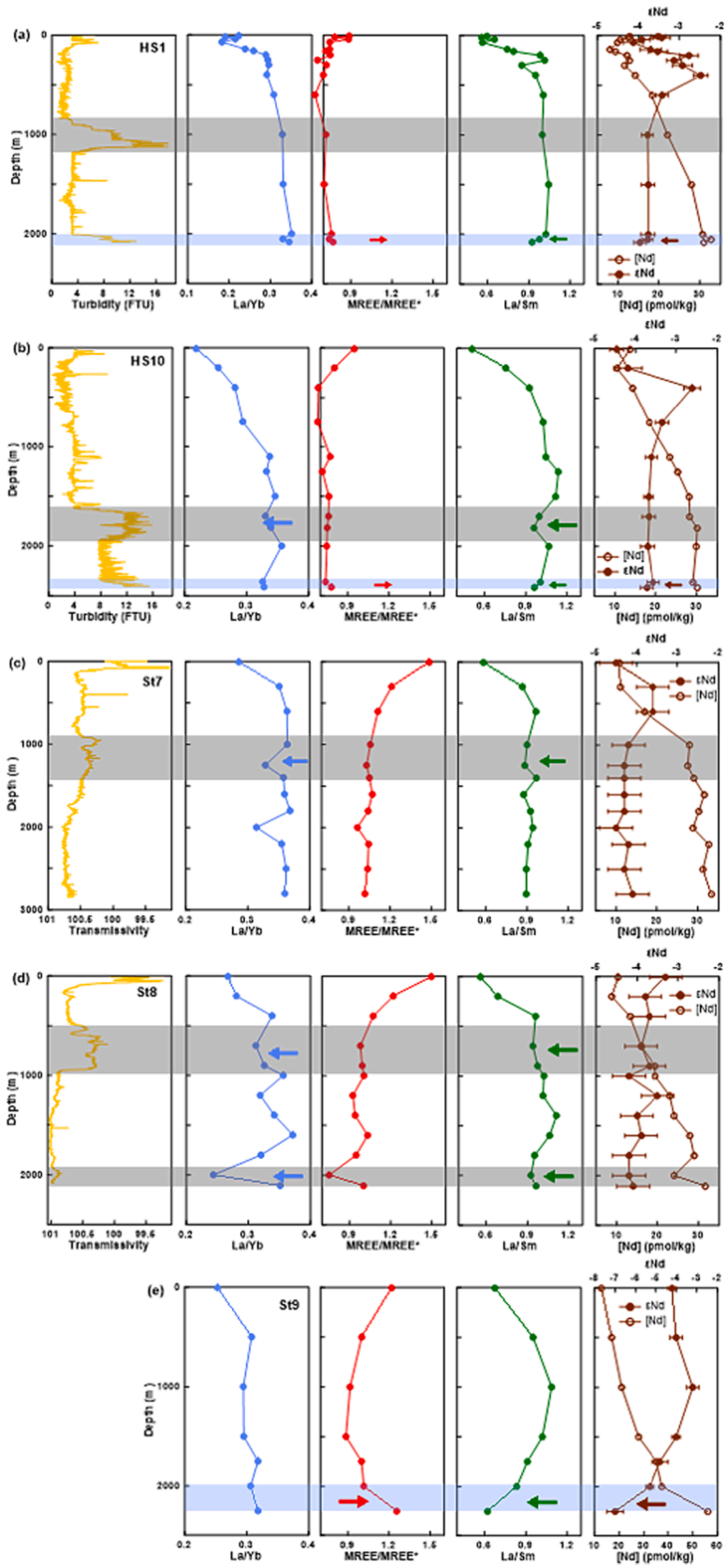

Fig. 9. Vertical profiles of turbidity (yellow line), La/Yb (blue dots), MREE* (red dots). La/Sm (green dots) and Nd concentrations (brown circles) and isotopic compositions (brown dots) in stations HS1, HS10, St7, St8 and St9. Grey and blue shallow squares highlight the nepheloid layers and bottom turbidity intervals, respectively.

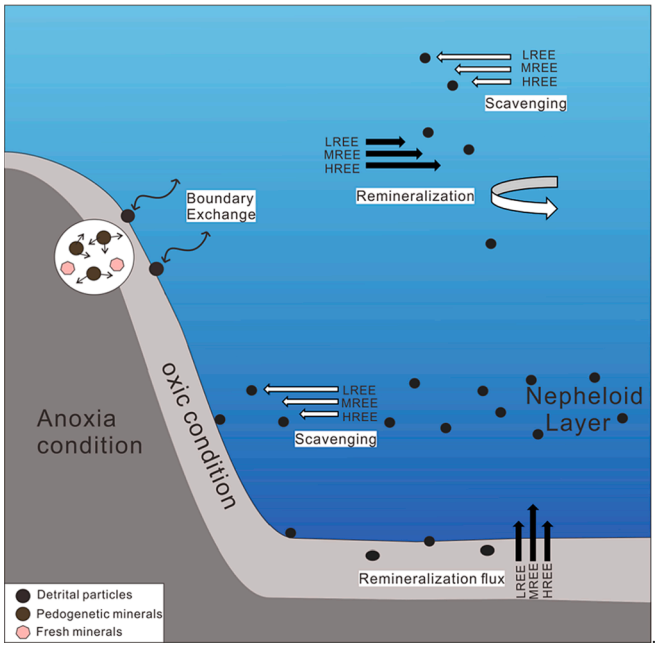

Fig. 10. Simplified schematic diagram of dissolved REE cycle in seawater.

As the NPIW flows into the SCS via the Luzon Strait, stations HS1 and HS10, located off the southwest coast of Taiwan, record its "original" εNd values (Fig. 11c) because of the low efficiency of primary minerals like illite to exchange Nd with seawater. But as the NPIW progresses along the eastern margin of China (St7, St8 and St9), increasing inputs of pedogenic minerals induce additional lithogenic Nd, which is characterized by an unradiogenic signature, and significantly modify the εNd values of the intermediate water masses from −2.5 to −3.8 (Fig. 11c). Although the specific impact of mineralogy on the boundary exchange of Nd needs further validation by field experiments, it seems that Nd from sediments that have undergone chemical weathering are more easily exchanged with Nd from seawater rather than the Nd from sediments that have undergone physical erosion (Fig. 10).

5.5. *The role of benthic nepheloid layers versus benthic flux*

Benthic nepheloid layers are present at the bottom of the three water stations HS1, HS6 and HS10, as observed from the vertical transmissivity (Fig. 9). We note that seawater samples and CTD data for stations St7 and St8 are not available for the deepest depth of the water column. Thus, no benthic nepheloid layers have been observed at the bottom of these stations which means that they cannot provide any information regarding interactions between deep-sea sediments and seawater.

It has been shown that suspended sediment concentrations of >0.5 mg/L are delivered from Taiwanese rivers (eg. Gaoping River) directly into the deep ocean, mainly during Typhoon events in the Gaoping canyon (Zhang et al., 2018). As in other nepheloid layers within the water column, bottom scavenging seems to affect the REE content and fractionation of bottom water, as is widely observed in the South Atlantic (Casse et al., 2019). The fact that the La/Sm ratio decreases while the La/Yb ratio remains unchanged in the benthic nepheloid layers at station St9 (Figs. 5 and 9), indicates a pronounced enrichment of MREEs compared to LREEs and HREEs. MREE enrichment at the bottom of St9 contrasts with the vertical distributions of MREE in the intermediate nepheloid layers observed in the water column (Fig. 9). In this case, a flux from lower sediments in anoxic layers, which contain more MREE compared to LREE and HREE, provides a reasonable explanation for the distribution of dissolved REE concentrations observed at the bottom of these stations (Fig. 10). The re-mineralization of oxides in anoxic layer sediments just below sediments interface may release abundant REEs to pore water (Haley et al., 2004; Deng et al., 2017), since the MREEs display a peculiar affinity towards manganese oxides (Bayon et al., 2004; Pattan et al., 2005). It is likely that the remineralization flux from the degradation of particles (authigenic manganese oxides and/or phosphates) results in the transfer of MREE-enriched signals to pore water resulting, in turn, in MREE enrichment in the uppermost pore waters (Deng et al., 2017; Du et al., 2022; Creac'h et al., 2023). A fraction of REEs is likely to diffuse to benthic water and, as originally indicated here by our results, subsequently causes an

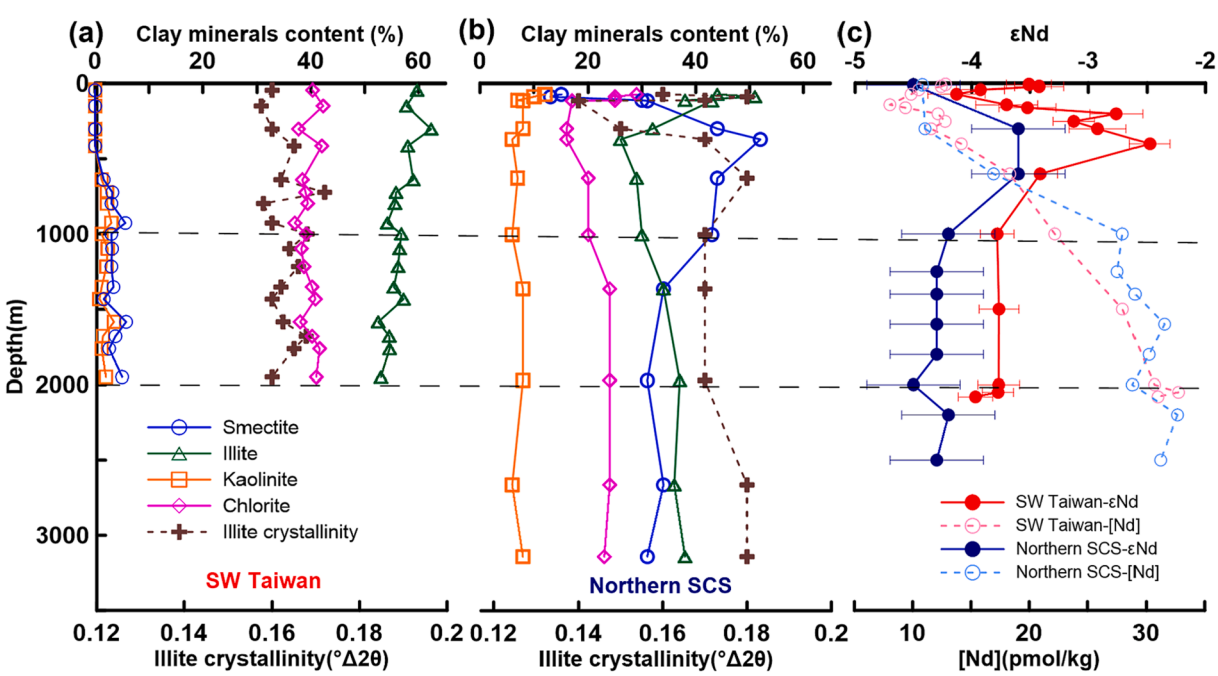

Fig. 11. Clay mineral distributions along depth transects off southwestern Taiwan (a; Liu et al., 2010) and northern SCS (b; Liu et al., 2010). (c) Nd isotopic compositions and concentrations of HS1 southwest of Taiwan and St7 in northern SCS (results of St7 are from Wu et al., 2015).

increase in the MREE/MREE* ratio of bottom seawater. Overall, the potential benthic flux carrying MREEs greatly impacts the REE fractionation of the bottom of St9.

In addition, at the bottom of stations St9, the εNd values are more negative than in the shallower waters of these stations. As we discussed above, the resuspended particles in nepheloid layers seem not to greatly change the Nd isotope compositions of seawater, thus the potential Nd sources must be the subsurface sediments. We take St9, which displays a significant εNd excursion, as an example to calculate the Nd isotopic compositions of the added Nd sources. The mass balance calculations would be:

$$\varepsilon_{Nd}^{original} * [Nd]_{original} + \varepsilon_{Nd}^{add} * [Nd]_{add} = \varepsilon_{Nd}^{final} * [Nd]_{final}$$

We use the water masses at similar depth (2200 m) in the nearby station St7 as original water masses from lateral advection for St9 (2250 m), then all the Nd added from the benthic flux is $[Nd]_{add} = [Nd]_{St9}$-$[Nd]_{St7}$. Thus, the calculated ε_{Nd}^{add} is -10.9 ± 1.1, which corresponds to the Nd isotopic signature of surface sediments in the northwestern margin of the SCS (from ~-9.3 to −11.8, Liu et al., 2016). This suggests that the early diagenesis of subsurface sediments may preferentially release Nd with the same isotopic signature as the deep-sea sediments. This process is different from the scavenging effect observed in the nepheloid layers within the water column. Our results support the idea that benthic flux may significantly affect the Nd isotope compositions of bottom seawater (Abbott et al., 2015).

For stations HS1 and HS10, the bottom water displays a slight negative excursion and no increase in Nd concentration. Considering the occurrence of benthic nepheloid layers, a scavenging process might decrease the Nd added from benthic flux but attenuate the modification of Nd isotopes. In addition, the mineralogical composition of the margin of South Taiwan mainly consists of minerals resulting from physical erosion which should be less reactive to Nd exchange with pore water and seawater than sediments on the eastern margin of China (station St9).

An adapted sampling strategy of seawater at the sediment interface and pore water is encouraged, and further investigations on the major and trace element of these fluids would undoubtedly help us gain a better understanding of benthic flux in the northern SCS.

6. Conclusions

Three vertical profiles of dissolved REE concentrations and Nd isotope compositions from water stations close to Taiwanese deep-sea canyons have been analyzed and combined with previous REE results obtained from 16 stations located in the Northern SCS. The aim is to evaluate the impact of intermediate and benthic nepheloid layers and of contrasted mineralogical sediment compositions of the margin of southern Taiwan and the eastern margin of China on dissolved REE concentrations and εNd distributions. We conclude that:

1/ The Nd isotope compositions of seawater reflect the advection of water masses from the western Pacific Ocean to the northern SCS. The surface seawater of the northern SCS yields a εNd value that is slightly less radiogenic than NPTW values, thus indicating a modification of Nd isotopic composition by lithogenic input from Taiwan's rivers. At intermediate depth, the most radiogenic value (εNd = −2.48) was found at around 400 m off southern Taiwan and results from an inflow of NPIW through the northern part of the Luzon Strait. Below 1500 m, the εNd values in the SCS are identical to PDW εNd values recorded in the Philippine Sea.

2/ Intermediate water at a greater distance from the Luzon Strait (margin of eastern China) shows a negative εNd value resulting from the upwelling of less radiogenic deep-water of the SCS, as well as boundary exchange with unradiogenic continental sediments. We have shown that intermediate water (from 300 to 800 m water depth) becomes less radiogenic along the margin of eastern China due to Nd exchange of seawater with unradiogenic sediments (from −10.2 to −12.6) deriving from the tropical soils of Chinese river basins. We have proposed that pedogenetic minerals from Chinese tropical soils modify the Nd isotopic compositions of seawater more efficiently than fresh detrital minerals resulting from very high physical erosion rates on Taiwan Island.

3/ In the nepheloid layers, scavenging of suspended particles greatly impact the REE fractionation in this layer. However, Nd isotope compositions do not show any significant change compared to neighboring layers. In contrast, a remineralization flux from particle degradation could play a role in the dissolved REE concentrations at the bottom, and this process causes a slight negative shift in the εNd values of the bottom water. The exact mechanism of this remineralization flux requires further investigation of the REE and Nd isotopes of pore water of sediments in the studied area.

Declaration of Competing Interest

The authors declare that they have no known competing financial interests or personal relationships that could have appeared to influence the work reported in this paper.

Acknowledgements

We thank the IFREMER (Institut Polaire Emile Victor), the crews and scientific teams of the HYDROSED research cruise for their excellent work during the seawater sampling. Y. Huang acknowledges the CSC for supporting her study in France. We gratefully acknowledge the assistance provided by Louise Bordier during Nd isotope analyses. We especially thank three anonymous reviewers for their constructive reviews, which significantly helped to improve this manuscript.

Appendix A. Supplementary material

Supplementary material includes three supplemental figures and two tables. Figure S1 is the vertical profiles of dissolved REE concentrations at station HS1, HS6 and HS10; Figure S2 is the PAAS normalized REE patterns of three stations. Figure S3 is the PAAS-normalized REE pattern of surface water of the northern SCS (this study) and stations St2 and St3 in the Philippine Sea (Wu et al., 2015. Table S1 is the original data of seawater Nd isotope compositions (expressed as εNd), concentrations from this study along with hydrographic parameters. Table S2 is original data of seawater REE concentrations. Supplementary material to this article can be found online at https://doi.org/10.1016/j.gca.2023.08.026.

References

Abbott, A.N., 2019. A benthic flux from calcareous sediments results in non-conservative neodymium behavior during lateral transport: A study from the Tasman Sea. Geology 47, 363–366.
Abbott, A.N., Haley, B.A., McManus, J., 2015. Bottoms up: Sedimentary control of the deep North Pacific Ocean's εNd signature. Geology 43, 1035.
Abbott, A.N., Löhr, S.C., Payne, A., Kumar, H., Du, J., 2022. Widespread lithogenic control of marine authigenic neodymium isotope records? Implications for paleoceanographic reconstructions. Geochim. Cosmochim. Acta 319, 318–336.
Alibo, D.S., Nozaki, Y., 2000. Dissolved rare earth elements in the South China Sea: Geochemical characterization of the water masses. J. Geophys. Res. Oceans 105, 28771–28783.
Amakawa, H., Alibo, D.S., Nozaki, Y., 2000. Nd isotopic composition and REE pattern in the surface waters of the eastern Indian Ocean and its adjacent seas. Geochim. Cosmochim. Acta 64, 1715–1727.
Amakawa, H., Nozaki, Y., Alibo, D.S., Zhang, J., Fukugawa, K., Nagai, H., 2004. Neodymium isotopic variations in Northwest Pacific waters. Geochim. Cosmochim. Acta 68, 715–727.
Amakawa, H., Sasaki, K., Ebihara, M., 2009. Nd isotopic composition in the central North Pacific. Geochim. Cosmochim. Acta 73, 4705–4719.
Arsouze, T., Dutay, J.-C., Lacan, F., Jeandel, C., 2009. Reconstructing the Nd oceanic cycle using a coupled dynamical – biogeochemical model. Biogeosciences 6, 2829–2846.

Bayon, G., German, C.R., Burton, K.W., Nesbitt, R.W., Rogers, N., 2004. Sedimentary Fe–Mn oxyhydroxides as paleoceanographic archives and the role of aeolian flux in regulating oceanic dissolved REE. Earth Planet. Sci. Lett. 224, 477–492.
Behrens, M.K., Pahnke, K., Schnetger, B., Brumsack, H.-J., 2018. Sources and processes affecting the distribution of dissolved Nd isotopes and concentrations in the West Pacific. Geochim. Cosmochim. Acta 222, 508–534.
Bertram, C.J., Elderfield, H., 1993. The geochemical balance of the rare earth elements and neodymium isotopes in the oceans. Geochim. Cosmochim. Acta 57, 1957–1986.
Blaser, P., Gutjahr, M., Pöppelmeier, F., Frank, M., Kaboth-Bahr, S., Lippold, J., 2020. Labrador Sea bottom water provenance and REE exchange during the past 35,000 years. Earth Planet. Sci. Lett. 542, 116299.
Broecker, W.S., Patzert, W.C., Toggweiler, J.R., Stuiver, M., 1986. Hydrography, chemistry, and radioisotopes in the Southeast Asian basins. J. Geophys. Res. 91, 14345–14354.
Broecker, W.S., Peng, T.-H., 1982. Tracers in the Sea. Cambirdge University Press.
Casse, M., Montero-Serrano, J.-C., St-Onge, G., Poirier, A., 2019. REE distribution and Nd isotope composition of estuarine waters and bulk sediment leachates tracing lithogenic inputs in eastern Canada. Mar. Chem. 211, 117–130.
Chao, S.Y., Shaw, P.Y., Wu, S.Y., 1996. Deep water ventilation in the South China Sea. Deep Sea Res. Part I 43, 445–466.
Chen, C.-T.-A., Wang, S.-L., Wang, B.-J., Pai, S.-C., 2001. Nutrient budgets for the South China Sea basin. Mar. Chem. 75, 281–300.
Chen, B., Wang, L., Song, S., Huang, B., Sun, J., Liu, H., 2011. Comparisons of picophytoplankton abundance, size, and fluorescence between summer and winter in northern South China Sea. Cont. Shelf Res. 31, 1527–1540.
Chung, C.-H., You, C.-F., Chu, H.-Y., 2009. Weathering sources in the Gaoping (Kaoping) river catchments, southwestern Taiwan: Insights from major elements, Sr isotopes, and rare earth elements. J. Mar. Syst. 76, 433–443.
Colin, C., Tisnérat-Laborde, N., Mienis, F., Collart, T., Pons-Branchu, E., Dubois-Dauphin, Q., Frank, N., Dapoigny, A., Ayache, M., Swingedouw, D., Dutay, J., Eynaud, F., Debret, M., Blamart, D., Douville, E., 2019. Millennial-scale variations of the Holocene North Atlantic mid-depth gyre inferred from radiocarbon and neodymium isotopes in cold water corals. Quat. Sci. Rev. 211, 93–106.
Copard, K., Colin, C., Douville, E., Freiwald, A., Gudmundsson, G., De-Mol, B., Frank, N., 2010. Nd isotopes in deep-sea corals in the North-eastern Atlantic. Quat. Sci. Rev. 29, 2499–2508.
Creac'h, L., Noble, T., Chase, T., Charlier, B., Townsend, A., Perez-Tribouillier, H., Dietz, C., 2023. Unradiogenic reactive phase controls the εNd of authigenic phosphates in East Antarctic margin sediment. Geochim. Cosmochim. Acta 344, 190–206.
Dadson, S.J., Hovius, N., Chen, H., Dade, W.B., Hsieh, M.L., Willett, S.D., Hu, J.-C., Horng, M.J., Chen, M.C., Stark, C.P., Lague, D., Lin, J.C., 2003. Links between erosion, runoff variability and seismicity in the Taiwan orogen. Nature 426, 648–651.
Deng, Y., Ren, J., Guo, Q., Cao, J., Wang, H., Liu, C., 2017. Rare earth element geochemistry characteristics of seawater and porewater from deep sea in western Pacific. Sci. Rep. 7, 16539.
Du, J., Haley, B.A., Mix, A.C., 2016. Neodymium isotopes in authigenic phases, bottom waters and detrital sediments in the Gulf of Alaska and their implications for paleo-circulation reconstruction. Geochim. Cosmochim. Acta 193, 14–35.
Du, J., Haley, B.A., Mix, A.C., Abbott, A.N., McManus, J., Vance, D., 2022. Reactive-transport modeling of neodymium and its radiogenic isotope in deep-sea sediments: The roles of authigenesis, marine silicate weathering and reverse weathering. Earth Planet. Sci. Lett. 596, 117792.
Dubois-Dauphin, Q., Colin, C., Bonneau, L., Montagna, P., Wu, Q., Van Rooij, D., Reverdin, G., Douville, E., Thil, F., Waldner, A., Frank, N., 2017. Fingerprinting Northeast Atlantic water masses using neodymium isotopes. Geochim. Cosmochim. Acta 210, 267–288.
Duhamel, M., Colin, C., Revel, M., Siani, G., Dapoigny, A., Douville, E., Wu, J., Zhao, Y., Liu, Z., Montagna, P., 2020. Variations in eastern Mediterranean hydrology during the last climatic cycle as inferred from neodymium isotopes in foraminifera. Quat. Sci. Rev. 237, 106306.
Fang, G., Wang, Y., Wei, Z., Fang, Y., Qiao, F., Hu, X., 2009. Interocean circulation and heat and freshwater budgets of the South China Sea based on a numerical model. Dyn. Atmos. Oceans 47, 55–72.
Frank, M., 2002. Radiogenic isotopes: Tracers of past ocean circulation and erosional input. Rev. Geophys. 40, 1.
Fuhr, M., Laukert, G., Yu, Y., Nürnberg, D., Frank, M., 2021. Tracing water mass mixing from the equatorial to the North Pacific Ocean with dissolved neodymium isotopes and concentrations. Front. Mar. Sci. 7, 603761.
Gan, J., Liu, Z., Hui, C.R., 2016. A Three-layer alternating spinning circulation in the South China Sea. J. Phys. Oceanogr. 46, 2309–2315.
Garcia-Solsona, E., Jeandel, C., 2020. Balancing rare earth element distributions in the Northwestern Mediterranean Sea. Chem. Geol. 532, 119372.
Gardner, W.D., Richardson, M.J., Mishonov, A.V., 2018. Global assessment of benthic nepheloid layers and linkage with upper ocean dynamics. Earth Planet. Sci. Lett. 482, 126–134.
Geng, M.H., Song, H.B., Guan, Y.X., Chen, J., 2018. Research on the distribution and characteristics of the nepheloid layers in the northern South China Sea by use of seismic oceanography method. Chin. J. Geophys. 61, 636–648.
Goldstein, S.L., Hemming, S.R., 2003. Long-lived isotopic tracers in oceanography, paleoceanography, and ice-sheet dynamics. Treatise Geochem. 6, 625.
Grasse, P., Bosse, L., Hathorne, E.C., Böning, P., Pahnke, K., Frank, M., 2017. Short-term variability of dissolved rare earth elements and neodymium isotopes in the entire water column of the Panama Basin. Earth Planet. Sci. Lett. 475, 242–253.
Grenier, M., Jeandel, C., Lacan, F., Vance, D., Venchiarutti, C., Cros, A., Cravatte, S., 2013. From the subtropics to the central equatorial Pacific Ocean: Neodymium isotopic composition and rare earth element concentration variations. J. Geophys. Res. Oceans 118, 592–618.
Grenier, M., Garcia-Solsona, E., Lemaitre, N., Trull, T.W., Bouvier, V., Nonnotte, P., van Beek, P., Souhaut, M., Lacan, F., Jeandel, C., 2018. Differentiating lithogenic supplies, water mass transport, and biological processes on and off the Kerguelen Plateau using rare earth element concentrations and neodymium isotopic compositions. Front. Mar. Sci. 5, 426.
Gutjahr, M., Frank, M., Stirling, C.H., Klemm, V., van de Flierdt, T., Halliday, A.N., 2007. Reliable extraction of a deepwater trace metal isotope signal from Fe–Mn oxyhydroxide coatings of marine sediments. Chem. Geol. 242, 351–370.
Haley, B.A., Klinkhammer, G.P., McManus, J., 2004. Rare earth elements in pore waters of marine sediments. Geochim. Cosmochim. Acta 68, 1265–1279.
Haley, B.A., Du, J., Abbott, A.N., McManus, J., 2017. The impact of benthic processes on rare earth element and neodymium isotope distributions in the oceans. Front. Mar. Sci. 4, 426.
Hindshaw, R.S., Aciego, S.M., Piotrowski, A.M., Tipper, E.T., 2018. Decoupling of dissolved and bedrock neodymium isotopes during sedimentary cycling. Geochem. Perspect. Lett. 8, 43–46.
Jeandel, C., 2016. Overview of the mechanisms that could explain the 'Boundary Exchange' at the land–ocean contact. Philos. Trans. R. Soc. London, Ser. A 374, 20150287.
Jeandel, C., Arsouze, T., Lacan, F., Téchiné, P., Dutay, J.C., 2007. Isotopic Nd compositions and concentrations of the lithogenic inputs into the ocean: A compilation, with an emphasis on the margins. Chem. Geol. 239, 156–164.
Jeandel, C., Delattre, H., Grenier, M., Pradoux, C., Lacan, F., 2013. Rare earth element concentrations and Nd isotopes in the Southeast Pacific Ocean. Geochem. Geophys. Geosyst. 14, 328–341.
Jia, Y., Tian, Z., Shi, X., Liu, J.P., Chen, J., Liu, X., Ye, R., Ren, Z., Tian, J., 2019. Deep-sea sediment resuspension by internal solitary waves in the northern South China Sea. Sci. Rep. 9, 12137.
Kawabe, M., Fujio, S., Yanagimoto, D., Tanaka, K., 2009. Water masses and currents of deep circulation southwest of the Shatsky Rise in the western North Pacific. Deep-Sea Res. I 56, 1675–1687.
Kawabe, M., Fujio, S., 2010. Pacific Ocean circulation based on observation. J. Ocean. 66, 389–403.
Lacan, F., Jeandel, C., 2001. Tracing Papua new guinea imprint on the central Equatorial Pacific Ocean using neodymium isotopic compositions and rare earth elemen patterns. Earth Planet. Sci. Lett. 186, 497–512.
Lacan, F., Jeandel, C., 2005. Neodymium isotopes as a new tool for quantifying exchange fluxes at the continent–ocean interface. Earth Planet. Sci. Lett. 232, 245–257.
Larkin, C.S., Piotrowski, A.M., Hindshaw, R.S., Bayon, G., Hilton, R.G., Baronas, J.J., Dellinger, M., Wang, R., Tipper, E.T., 2021. Constraints on the source of reactive phases in sediment from a major Arctic river using neodymium isotopes. Earth Planet. Sci. Lett. 565, 116933.
Li, L., Qu, T., 2006. Thermohaline circulation in the deep South China Sea basin inferred from oxygen distributions. J. Geophys. Res. 111, C05017.
Li, C.-S., Shi, X.-F., Kao, S.-J., Liu, Y.-G., Lyu, H.-H., Zou, J.-J., Liu, S.-F., Qiao, S.-Q., 2013. Rare earth elements in fine-grained sediments of major rivers from the high-standing island of Taiwan. J. Asian Earth Sci. 69, 39–47.
Liu, Z., Colin, C., Li, X., Zhao, Y., Tuo, S., Chen, Z., Siringan, F.P., Liu, J.T., Huang, C.-Y., You, C.-F., Huang, K.-F., 2010. Clay mineral distribution in surface sediments of the northeastern South China Sea and surrounding fluvial drainage basins: Source and transport. Mar. Geol. 277, 48–60.
Liu, J.T., Hsu, R.T., Hung, J.J., Chang, Y.P., Wang, Y.H., Rendle-Bühring, R.H., Lee, C.L., Huh, C.A., Yang, R.J., 2016a. From the highest to the deepest: The Gaoping River-Gaoping Submarine Canyon dispersal system. Earth Sci. Rev. 153, 274–300.
Liu, Z., Tuo, S., Colin, C., Liu, J.T., Huang, C.-Y., Selvaraj, K., Chen, C.T.A., Zhao, Y., Siringan, F.P., Boulay, S., Chen, Z., 2008. Detrital fine-grained sediment contribution from Taiwan to the northern South China Sea and its relation to regional ocean circulation. Mar. Geol. 255, 149–155.
Liu, Z., Zhao, Y., Colin, C., Stattegger, K., Wiesner, M.G., Huh, C.-A., Zhang, Y., Li, X., Sompongchaiyakul, P., You, C.-F., Huang, C.-Y., Liu, J.T., Siringan, F.P., Le, K.P., Sathiamurthy, E., Hantoro, W.S., Liu, J., Tuo, S., Zhao, S., Zhou, S., He, Z., Wang, Y., Bunsomboonsakul, S., Li, Y., 2016b. Source-to-sink transport processes of fluvial sediments in the South China Sea. Earth Sci. Rev. 153, 238–273.
McLennan, S.M., 1989. Rare earth elements in sedimentary rocks: influence of provence and sedimentary processes. Geochem. Mineral. Rare Earth Elements 21, 169–200.
Morrison, R., Waldner, A., Hathorne, E.C., Rahlf, P., Zieringer, M., Montagna, P., Colin, C., Frank, N., Frank, M., 2019. Limited influence of basalt weathering inputs on the seawater neodymium isotope composition of the northern Iceland Basin. Chem. Geol. 511, 358–370.
Nozaki, Y., Alibo, D.S., 2003. Importance of vertical geochemical processes in controlling the oceanic pro¢les of dissolved rare earth elements in the northeastern Indian Ocean. Earth Planet. Sci. Lett. 205, 155–172.
Pattan, J.N., Pearce, N.J.G., Mislankar, P.G., 2005. Constraints in using Cerium-anomaly of bulk sediments as an indicator of paleo bottom water redox environment: A case study from the Central Indian Ocean Basin. Chem. Geol. 221, 260–278.
Pham, V.Q., Grenier, M., Cravatte, S., Michael, S., Jacquet, S., Belhadj, M., Nachez, Y., Germineaud, C., Jeandel, C., 2019. Dissolved rare earth elements distribution in the Solomon Sea. Chem. Geol. 524, 11–36.
Piepgras, D.J., Wasserburg, G.J., 1980. Neodymium isotopic variations in seawater. Earth Planet. Sci. Lett. 50, 128–138.

Piotrowski, A.M., Goldstein, S.L., Hemming, S.R., Fairbanks, R.G., 2005. Temporal relationships of carbon cycling and ocean circulation at glacial boundaries. Science 307, 1933–1938.
Qu, T., Mitsudera, H., Yamagata, T., 1999. A climatology of the circulation and water mass distribution near the Philippine coast. J. Phys. Oceanogr. 29, 1488–1505.
Qu, T., Mitsudera, H., Yamagata, T., 2000. Intrusion of the North Pacific waters into the South China Sea. J. Geophys. Res. Oceans 105, 6415–6424.
Qu, T., Du, Y., Sasaki, H., 2006. South China Sea throughflow: A heat and freshwater conveyor. Geophys. Res. Lett. 33, L23617.
Rempfer, J., Stocker, T.F., Joos, F., Dutay, J.C., Siddall, M., 2011. Modelling Nd-isotopes with a coarse resolution ocean circulation model: Sensitivities to model parameters and source/sink distributions. Geochim. Cosmochim. Acta 75, 5927–5950.
Robinson, S., Ivanovic, R., van de Flierdt, T., Blanchet, C., Tachikawa, K., Martin, E., Cook, C., Williams, T., Gregoire, L., Plancherel, Y., Jeandel, C., Arsouze, T., 2021. Global continental and marine detrital εNd: An updated compilation for use in understanding marine Nd cycling. Chem. Geol. 567, 120119.
Robinson, S., Ivanovic, R., Gregoire, L., Tindall, J., van de Flierdt, T., Plancherel, Y., Pöppelmeier, F., Tachikawa, K., Valdes, P., 2023. Simulating marine neodymium isotope distributions using ND v1.0 coupled to the ocean component of the FAMOUS-MOSES1 climate model: sensitivities to reversible scavenging efficiency and benthic source distributions. Geosci. Model. Dev. 16, 1231–1264.
Sholkovitz, E.R., Shaw, T.J., Schneider, D.L., 1992. The geochemistry of rare earth elements in the seasonally anoxic water column and porewaters of Chesapeake Bay. Geochim. Cosmochim. Acta 56, 3389–3402.
Siddall, M., Khatiwala, S., van de Flierdt, T., Jones, K., Goldstein, S.L., Hemming, S., Anderson, R.F., 2008. Towards explaining the Nd paradox using reversible scavenging in an ocean general circulation model. Earth Planet. Sci. Lett. 274, 448–461.
Stichel, T., Hartman, A.E., Duggan, B., Goldstein, S.L., Scher, H., Pahnke, K., 2015. Separating biogeochemical cycling of neodymium from water mass mixing in the Eastern North Atlantic. Earth Planet. Sci. Lett. 412, 245–260.
Stichel, T., Kretschmer, S., Geibert, W., Lambelet, M., Plancherel, Y., Rutgers van der Loeff, M., van de Flierdt, T., 2020. Particle-Seawater Interaction of Neodymium in the North Atlantic. ACS Earth Space Chem. 4, 1700–1717.
Suga, T., Kato, A., Hanawa, K., 2000. North Pacific Tropical Water: its climatology and temporal changes associated with the climate regime shift in the 1970s. Prog. Oceanogr. 47, 223–256.
Tachikawa, K., Jeandel, C., Roy-Barman, M., 1999. A new approach to the Nd residence time in the ocean: the role of atmospheric inputs. Earth Planet. Sci. Lett. 170, 433–446.
Tachikawa, K., Athias, V., Jeandel, C., 2003. Neodymium budget in the modern ocean and paleo-oceanographic implications. J. Geophys. Res. 108, 3254.
Tachikawa, K., Arsouze, T., Bayon, G., Bory, A., Colin, C., Dutay, J.-C., Frank, N., Giraud, X., Gourlan, A.T., Jeandel, C., Lacan, F., Meynadier, L., Montagna, P., Piotrowski, A.M., Plancherel, Y., Pucéat, E., Roy-Barman, M., Waelbroeck, C., 2017. The large-scale evolution of neodymium isotopic composition in the global modern and Holocene ocean revealed from seawater and archive data. Chem. Geol. 457, 131–148.
Tanaka, T., Togashi, S., Kamioka, H., Amakawa, H., Kagami, H., Hamamoto, T., Yuhara, M., Orihashi, Y., Yoneda, S., Shimizu, H., Kunimaru, T., Takahashi, K., Yanagi, T., Nakano, T., Fujimaki, H., Shinjo, R., Asahara, Y., Tanimizu, M., Dragusanu, C., 2000. JNdi-1: a neodymium isotopic reference in consistency with LaJolla neodymium. Chem. Geol. 168, 279–281.
Tharaud, M., Gardoll, S., Khelifi, O., Benedetti, M.F., Sivry, Y., 2015. uFREASI: user-FRiendly Elemental dAta procesSIng. A free and easy-to-use tool for elemental data treatment. Microchem. J. 121, 32–40.
Tian, Z., Liu, Y., Zhang, X., Zhang, Y., Zhang, M., 2022. Formation mechanisms and characteristics of the marine nepheloid layer: A Review. Water 14, 678.
Tian, J., Yang, Q., Liang, X., Xie, L., Hu, D., Wang, F., Qu, T., 2006. Observation of Luzon Strait transport. Geophys. Res. Lett. 33, L19607.
Tian, J., Zhao, W., Yang, Q., 2009. Enhanced diapycnal mixing in the South China Sea. J. Phys. Oceanogr. 39, 3191–3203.
van de Flierdt, T., Pahnke, K., Amakawa, H., Andersson, P., Basak, C., Coles, B., Colin, C., Crocket, K., Frank, M., Frank, N., Goldstein, S.L., Goswami, V., Haley, B.A., Hathorne, E.C., Hemming, S.R., Henderson, G.M., Jeandel, C., Jones, K., Kreissig, K., Lacan, F., Lambelet, M., Martin, E.E., Newkirk, D.R., Obata, H., Pena, L., Piotrowski, A.M., Pradoux, C., Scher, H.D., Schöberg, H., Singh, S.K., Stichel, T., Tazoe, H., Vance, D., Yang, J., 2012. GEOTRACES intercalibration of neodymium isotopes and rare earth element concentrations in seawater and suspended particles. Part 1: reproducibility of results for the international intercomparison. Limnol. Oceanogr. Methods 10, 234–251.
van de Flierdt, T., Griffiths, A.M., Lambelet, M., Little, S.H., Stichel, T., Wilson, D.J., 2016. Neodymium in the oceans: a global database, a regional comparison and implications for palaeoceanographic research. Philos. Trans. R. Soc. London, Ser. A 374, 20150293.
von Blanckenburg, F., Nägler, T.F., 2001. Weathering versus circulation-controlled changes in radiogenic isotope tracer composition of the Labrador Sea and North Atlantic Deep Water. Paleoceanography 16, 424–434.
Wang, R., Clegg, J.A., Scott, P.M., Larkin, C.S., Deng, F., Thomas, A.L., Zheng, X.Y., Piotrowski, A.M., 2021. Reversible scavenging and advection – Resolving the neodymium paradox in the South Atlantic. Geochim. Cosmochim. Acta 314, 121–139.
Wang, R., Williams, T.J., Hillenbrand, C.D., Ehrmann, W., Larkin, C.S., Hutchings, A.M., Piotrowski, A.M., 2022. Boundary processes and neodymium cycling along the Pacific margin of West Antarctica. Geochim. Cosmochim. Acta 327, 1–20.
Wang, G., Xie, S.-P., Qu, T., Huang, R.X., 2011. Deep South China Sea circulation. Geophys. Res. Lett. 38, L05601.
Wei, G., Liu, Y., Ma, J., Xie, L., Chen, J., Deng, W., Tang, S., 2012. Nd, Sr isotopes and elemental geochemistry of surface sediments from the South China Sea: Implications for Provenance Tracing. Mar. Geol. 319–322, 21–34.
Wilson, D.J., Piotrowski, A.M., Galy, A., McCave, I.N., 2012. A boundary exchange influence on deglacial neodymium isotope records from the deep western Indian Ocean. Earth Planet. Sci. Lett. 341–344, 35–47.
Wu, Q., Colin, C., Liu, Z., Douville, E., Dubois-Dauphin, Q., Frank, N., 2015. New insights into hydrological exchange between the South China Sea and the Western Pacific Ocean based on the Nd isotopic composition of seawater. eep Sea Res. Part II. 122, 25–40.
Wu, Q., Colin, C., Liu, Z., Bassinot, F., Dubois-Dauphin, Q., Douville, E., Thil, F., Siani, G., 2017. Foraminiferal εNd in the deep north-western subtropical Pacific Ocean: Tracing changes in weathering input over the last 30,000 years. Chem. Geol. 470, 55–66.
Wu, Q., Liu, Z., Colin, C., Douville, E., Zhao, Y., Wu, J., Dapoigny, A., Bordier, L., Ma, P., Huang, Y., 2022. Dissolved rare earth element and neodymium isotope distributions in the South China Sea: Water mass source versus particle dissolution. Front. Mar. Sci. 9, 1003749.
Wyrtki, K., 1961. Physical Oceanography of the Southeast Asian Waters. University of California.
Xie, L., Tian, J., Zhang, S., Zhang, Y., Yang, Q., 2011. An anticyclonic eddy in the intermediate layer of the Luzon Strait in Autumn 2005. J. Oceanogr. 67, 37–46.
Yang, Q., Tian, J., Zhao, W., 2010. Observation of Luzon Strait transport in summer 2007. Deep Sea Res. Part I. 57, 670–676.
You, Y., 2003. The pathway and circulation of North Pacific Intermediate Water. Geophys. Res. Lett. 30, 2291.
Yu, Z., Colin, C., Douville, E., Meynadier, L., Duchamp-Alphonse, S., Sepulcre, S., Wan, S., Song, L., Wu, Q., Xu, Z., Bassinot, F., 2017a. Yttrium and rare earth element partitioning in seawaters from the Bay of Bengal. Geochem. Geophys. Geosyst. 18, 1388–1403.
Yu, Z., Colin, C., Meynadier, L., Douville, E., Dapoigny, A., Reverdin, G., Wu, Q., Wan, S., Song, L., Xu, Z., Bassinot, F., 2017b. Seasonal variations in dissolved neodymium isotope composition in the Bay of Bengal. Earth Planet. Sci. Lett. 479, 310–321.
Yuan, D., 2002. A numerical study of the South China Sea deep circulation and its relation to the Luzon Strait transport. Acta Oceanolog. Sinic. 21, 187–202.
Zhang, Y., Liu, Z., Zhao, Y., Colin, C., Zhang, X., Wang, M., Zhao, S., Kneller, B., 2018. Long-term in situ observations on typhoon-triggered turbidity currents in the deep sea. Geology 46, 675–678.
Zhao, Y., Liu, Z., Zhang, Y., Li, J., Wang, M., Wang, W., Xu, J., 2015. In situ observation of contour currents in the northern South China Sea: Applications for deepwater sediment transport. Earth Planet. Sci. Lett. 430, 477–485.
Zhao, N., Oppo, D.W., Huang, K.F., Howe, J.N.W., Blusztajn, J., Keigwin, L.D., 2019. Glacial-interglacial Nd isotope variability of North Atlantic Deep Water modulated by North American ice sheet. Nat. Commun. 10, 5773.
Zhou, X., Zhan, T., Tan, N., Tu, L., Smol, J., Jiang, S., Zeng, F., Liu, X., Li, X., Liu, G., Liu, Y., Zhang, R., Shen, Y., 2023. Inconsistent patterns of Holocene rainfall changes at the East Asian monsoon margin compared to the core monsoon region. Quat. Sci. Rev. 301, 107952.
Zhu, Y., Sun, J., Wang, Y., Li, S., Xu, T., Wei, Z., Qu, T., 2019. Overview of the multi-layer circulation in the South China Sea. Prog. Oceanogr. 175, 171–182.